INTERNATIONAL JOURNAL OF CLIMATOLOGY, VOL. 17, 345–375 (1997)

AN ANALYSIS OF THE ENSO SIGNAL IN THE TROPICAL ATLANTIC AND WESTERN INDIAN OCEANS

SHARON E. NICHOLSON
Florida State University, Department of Meteorology, Tallahassee, FL 32306, USA
email: sen@huey.met.fsu.edu
Received 30 August 1995
Revised 20 July 1996
Accepted 25 July 1996

ABSTRACT

This article examines the time–space evolution of the El Niño-Southern Oscillation (ENSO) signal in the tropical Atlantic and western Indian Oceans, using harmonic analysis. Composites of sea-surface temperatures (SSTs) and other variables are examined for a 24-month period beginning 6 months prior to the year of maximum warming in the Pacific (termed year 0). An ENSO signal is apparent in the Atlantic in six out of eight Pacific episodes and in the Indian Ocean in all eight episodes. Warming begins along the south-eastern Atlantic coast early in year 0, some months later elsewhere in the Atlantic and in the Indian Ocean. Maximum warming occurs in the Atlantic in October–December of year 0, but in the following January–March in the Indian Ocean.

In these oceans a 'cold' phase occurs synchronously with the first half of the Pacific episode (July of year -1 to June of year 0, in the Rasmusson–Carpenter terminology), a 'warm' phase with the second half. Maximum cooling is 1 year prior to maximum warming in both oceans. In the Atlantic the cold phase occurs most consistently; in the Indian Ocean the warm phase occurs most consistently. There is a season-by-season reversal of SST anomalies and, to a lesser extent, pressure anomalies between the cold and warm phases. This is the basis for the biennial component of the ENSO signal.

Our results indicate that the ENSO signal in African rainfall variability is a manifestation of ENSO's influence on SSTs in the Atlantic and Indian Oceans and, in turn, their influence on rainfall. The cold and warm phases correspond roughly to enhanced and reduced rainfall over the African continent, respectively. A similar reversal of rainfall anomalies is apparent season-by-season during these phases. The timing of the warming and cooling is relatively constant in the Indian Ocean. However, the onset of the warming and cooling in the south and equatorial Atlantic occurs progressively later from south to north, thus the signal 'propagates' northward. A similar propagation, synchronous in timing and latitude, is evident in ENSO induced rainfall anomalies over southern and equatorial Africa during the 'cold' phase but not during the 'warm' phase. This may be indicative of a switch in the control of rainfall from the Atlantic Ocean to the Indian Ocean during these phases.
 Int. J. Climatol. 17, 345–375 (1997)

(No. of Figs: 24 No. of Tables: 2 No. of Refs: 77)

KEY WORDS: ENSO; tropical Atlantic Ocean; Indian Ocean; harmonic analysis; sea surface temperature anomalies

INTRODUCTION

The El Niño–Southern Oscillation (ENSO) phenomenon has been studied largely in the context of the Pacific Ocean and adjacent regions, although research has long established that it is a global-scale phenomenon (Horel and Wallace, 1981; Arkin, 1982; Barnett, 1983; Yasunari, 1985). World-wide teleconnections in rainfall have been established (e.g. Ropelewski and Halpert, 1987,1989; Kiladis and Diaz, 1989). These include areas of eastern Africa, where most ENSO events produce abnormally high rainfall, and much of southern Africa, where the likely consequence of ENSO is drought (Lindesay *et al.*, 1986; Nicholson and Entekhabi, 1986,1987; van Heerden *et al.*, 1988). These regions are also strongly influenced by the Atlantic and Indian Oceans (Nicholson and Entekhabi, 1987; Walker, 1990), and the question arises as to whether the ENSO influence in this region is actually manifested through its effects in the Atlantic and Indian Oceans.

A number of observations suggest that ENSO episodes trigger large-scale changes in the tropical Atlantic and western Indian Oceans. The dominant time-scale of sea-surface temperature (SST) fluctuations in tropical sectors

CCC 0899-8418/97/040345-31 $17.50

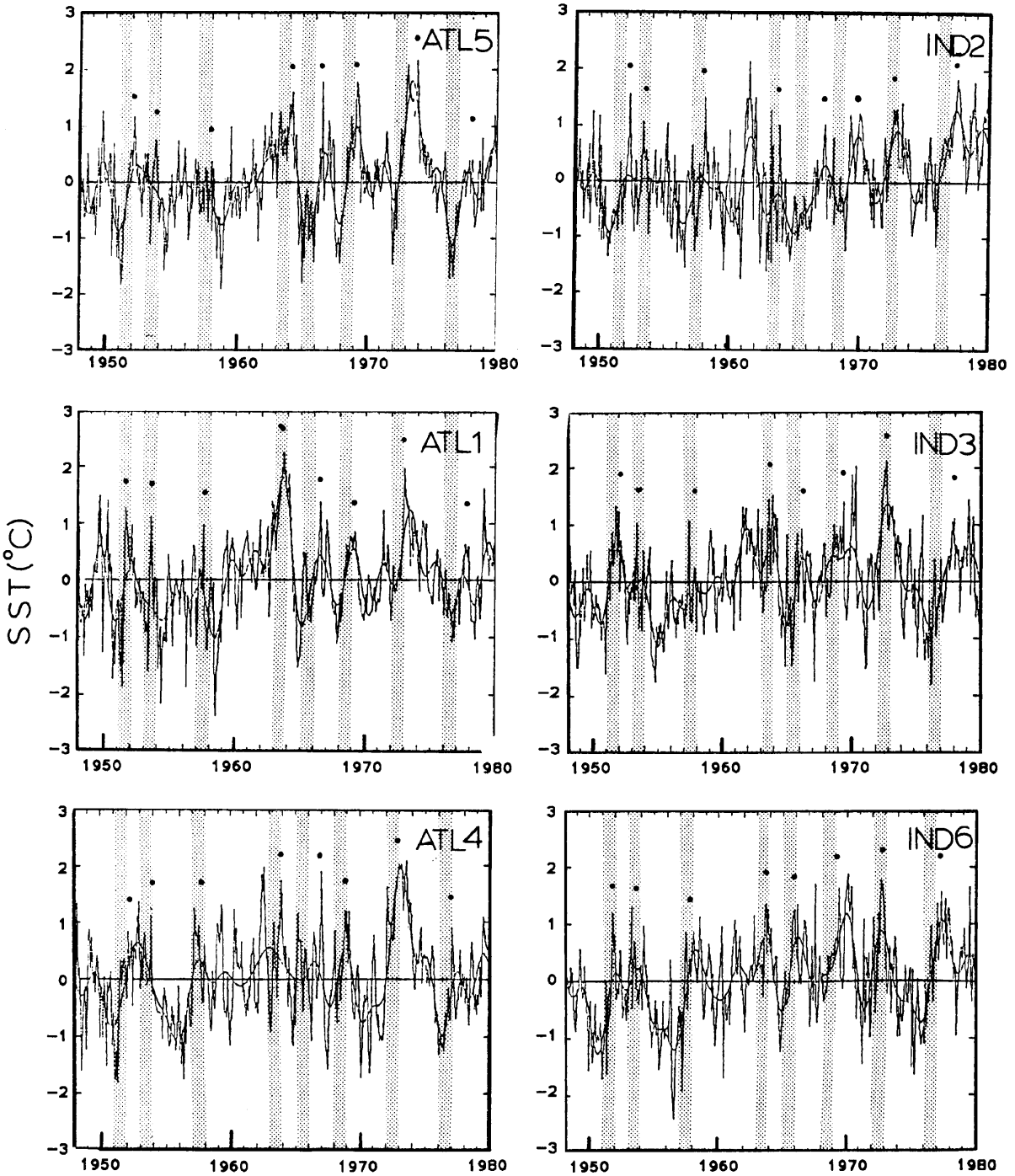

Figure 1. The SST anomaly series for various Atlantic and Indian Ocean sectors (from Nicholson *et al.*, 1988). ENSO years (year 0) are shaded

of these oceans is 4 to 6 years, the same as for the Southern Oscillation (Nicholson and Nyenzi, 1990). Warming is apparent in most of these sectors during ENSO years (Figure 1). Large-scale Atlantic anomalies in association with ENSO have been demonstrated by Hastenrath and Heller (1977), Covey and Hastenrath (1978), Wolter (1987) and Aceituno (1988); Semazzi *et al.* (1988) also found an ENSO mode in Atlantic variability. Cadet (1985), Yasunari (1987a,b) and Tourre and White (1995) have demonstrated strong ENSO signals in SSTs in the Indian Ocean.

Areas of high SST variability in the Atlantic include the Gulf of Guinea and equatorial Atlantic to the south (Merle *et al.*, 1979) and the region of the Benguela current in the south-eastern Atlantic (Walker *et al.*, 1984; Shannon, 1985; Walker, 1987,1990). Warmings in upwelling regions in the Gulf of Guinea and off north-west Africa appear to be analogous to the Pacific ENSO and roughly correspond to it temporally (Hisard, 1980; Michelchen, 1985a,b). Anomalous warming occurs along the Benguela coast during most ENSO years (Gillooly and Walker, 1984; Nicholson and Entekhabi, 1987).

Interannual variability of SSTs appears to be remotely forced in these regions (Bakun, 1978; Michelchen, 1985b; Merle and Arnault, 1985; Shannon *et al.*, 1986; Walker, 1990). For example, the strength of the trades off north-east Brazil is correlated with SSTs and thermocline structure in the Gulf of Guinea (Servain *et al.*, 1982; Servain and Legler, 1986). A relaxation of the trades apparently induces a Kelvin-type wave to propagate along the Equator, elevating SSTs in that region and further south (Moore *et al.*, 1978; O'Brien *et al.*, 1978). However, Zebiak (1993) has recently demonstrated a strong relationship between pseudo-wind stress and SSTs in the equatorial Atlantic, suggesting a dynamic ocean–atmosphere coupling akin to ENSO.

Elsewhere in the tropical Atlantic, warm episodes have been demonstrated (e.g. Lamb *et al.*, 1986), but they appear to be somewhat out of phase with the Pacific ENSO. One such episode in 1984 followed the 1982–1983 Pacific ENSO (Horel *et al.*, 1986; Katz *et al.*, 1986; Philander, 1986; Hisard and Henin, 1987; Mechoso and Lyons, 1988). Maximum warming appears to have been achieved towards the end of the onset of ENSO (Hamilton and Allingham, 1988), i.e. during the 'mature phase' of ENSO (Rasmusson and Carpenter, 1982), and the mechanisms of warming are quite complex.

In this study, the ENSO signal in the tropical Atlantic and Indian Oceans is examined systematically, utilizing the analysis method applied by Ropelewski and Halpert (1986,1987,1989) to study ENSO's influence on global temperature and precipitation patterns. El Niño–Southern Oscillation composites of SSTs, surface winds and surface pressure are derived. Spectral analysis is also utilized to determine the coherence between time series of SSTs and the Southern Oscillation. The result is a complete description of the evolution of ENSO related warm episodes in the tropical Atlantic and western Indian Oceans. In a companion article, the relationship of these changes to African rainfall variability is examined (Nicholson and Kim, 1996).

2. DATA

The sea-surface temperature, wind and pressure data utilized in this study are that of the Comprehensive Ocean–Atmosphere Data Set (COADS) and cover the time period 1948 to 1988 (Woodruff *et al.*, 1987). The analysis sector extends from 40°N to 40°S and from the western Atlantic to the central Indian Ocean at about 100°E. The data consist of 'trimmed' monthly averages for $2^\circ \times 2^\circ$ squares, but here a $4^\circ \times 4^\circ$ grid has been utilized to facilitate computations. A previous study demonstrated that patterns of variability based on the 2° squares are essentially the same as those utilizing only 4° resolution (Nicholson and Nyenzi, 1990). The SST data are expressed as a 'normalized' anomaly, i.e. a departure from the long-term mean divided by the standard departure, for the primary analyses.

The COADS data set has been used in many studies of marine surface variables and has proven to provide reliable estimates of temperature, wind and surface pressure (e.g. Deser and Wallace, 1990; Ward, 1992; Nigam and Shen, 1993; Allan *et al.*, 1995). The data set contains two biases produced by changes in observational practices. The first involves SST estimates based on 'bucket' or engine-cooling water intake data and the second involves the use of anemometer readings versus Beaufort force estimates of wind speed. The number of ships utilizing the 'intake' water to measure SSTs increased markedly in the 1940s. For this reason, and because the number of reports increases dramatically following World War II, our analysis begins in 1948. The use of anemometer readings relative to Beaufort force estimates also increased since that time, producing an increasing

trend in wind speed since the late 1940s (Cardone *et al.*, 1990). In view of this, the prescribed method of Ward (1992) is used to correct wind data from 1949 onward.

3. METHODOLOGY

The goal of this study is to describe the characteristic manifestations of a Pacific ENSO episode in the tropical Atlantic and western Indian Oceans. This is done by way of a composite of all ENSO episodes occurring during the period 1948 to 1988. However, the analysis is complicated by several factors. First of all, an abrupt change in the basic state of the coupled ocean–atmosphere system appears to have occurred in the late 1970s (Graham, 1994), some aspects of which resemble an ENSO episode. Although this was documented mainly for the Pacific, a scan of the data for the Atlantic and Indian Oceans suggests a similar shift at the same time. Also, the 1982 and 1987 ENSO episodes are quite unlike earlier episodes in terms of such characteristics as timing, intensity and duration (Gill and Rasmusson, 1983; Rasmusson and Mo, 1993). It is felt therefore that the 'typical' Atlantic and Indian Ocean response to ENSO is identified best using data prior to the climatic shift of the late 1970s. For this reason, we have chosen to analyse mainly episodes occurring during the period up to 1979 and to do a cursory examination of the two subsequent ENSO episodes and compare them with the results of the longer period. The primary analysis period, 1948–1979, is comparable to that of several recent papers studying global ENSO (e.g. Deser and Wallace, 1990; Ropelewski *et al.*, 1992).

The first step of the methodology is to describe a 'composite' ENSO episode. The choice of years is not straightforward, because various authors disagree as to the appropriate years to include as ENSO episodes. Nevertheless, episodes defined on the basis of low values of the Southern Oscillation Index (e.g. Ropelewski and Jones, 1987) are in relatively good agreement with Pacific warm events (e.g. Rasmusson and Carpenter, 1982; Deser and Wallace, 1990). Most discrepancies involve 2-year episodes, such as 1968–1969 and 1976–1977, in which the warming began before the strong decline in the SOI (Schonher and Nicholson, 1989). In this study the first year of such events is used to define ENSO episodes.

Following the convention of Rasmusson and Carpenter (1982), an episode is defined as the 2-year period commencing in July prior to the year in which the maximum ENSO warming in the Pacific occurs, designated as July (−1). Months in the year of maximum ENSO Pacific anomalies are designated as (0), those in the following year as (+1). Both monthly and seasonal SST, wind and sea-level pressure composite-averages for each grid-square are calculated. This represents the temporal evolution of surface variables in the Atlantic and Indian Oceans during a 'typical' Pacific ENSO. This composite is described in Section 4.

The ENSO signal is detected using the methodology established by Ropelewski and Halpert (1986). A standard harmonic analysis (section 5) is performed on the resulting 24-point, monthly, ENSO-composite SST time series for each grid-square. The phase and amplitude of the first harmonic are used to represent, respectively, the time of maximum warming in each grid-square and the total magnitude of the temperature variation during the 2-year period. Vectors representing the phase and amplitude at each grid-point, as illustrated in Figure 2, are plotted on a map.

From this map, ocean sectors that appear to have a coherent ENSO signal are selected subjectively. Then the coherence within these sectors is assessed, following Ropelewski and Halpert (1986), from the ratio of the vector and scalar magnitudes of the harmonics averaged over all grid-squares in the sectors. That study considered areas within which this ratio exceeds 0·80 to be coherent with respect to SST variability within ENSO episodes. In view of the smaller number episodes in this study, the criteria is set at 0·90. For each of these sectors time series of SSTs are derived, with the value at each point in time calculated as the arithmetic average of the values at all grid-points within each sector deemed coherent. This is a 24-month ENSO 'aggregate' response for the sector.

These 24-month time series are examined in order to ensure that SST anomalies of the same sign persisted for multi-month periods and to identify the 'seasons' within the ENSO cycle with the largest apparent response. For each sector, both the 3-month period of maximum positive anomalies and of maximum negative anomalies are determined. The SST time series for each of these 'seasons' is derived for the period 1948 to 1988 as the anomaly averaged over all grid-points within the sector. These seasonal time series indicate the consistency of the response associated with ENSO; areas for which the time series indicate anomalies of the same sign in six or more of the eight ENSO episodes between 1948 and 1988 are considered to have robust ENSO signals.

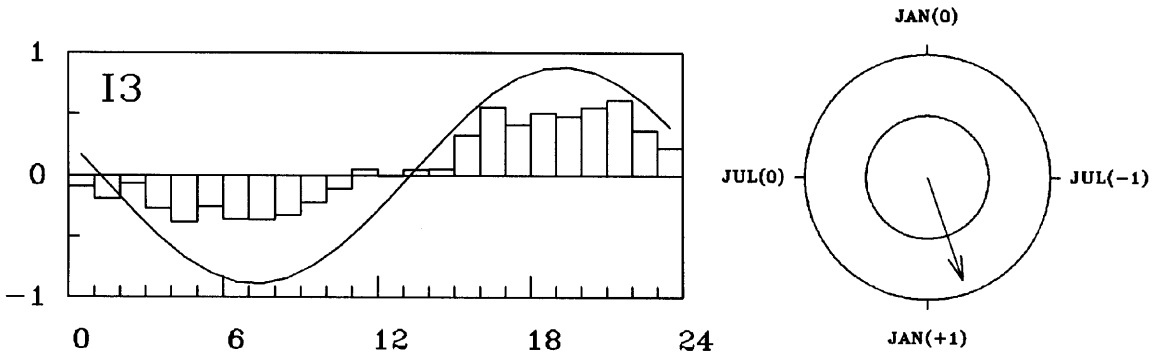

Figure 2. Key to the depiction of SST fluctuations via harmonic analysis. The time series represents an SST anomaly averaged over all grid-points in the chosen sector and over all eight ENSO events in the period 1948 to 1979. The (−1, 0, +1) refer to months in the years prior to, during, and following a Pacific ENSO event. The data are standardized, so that the amplitude refers to standard deviations. The harmonic dial illustrates the vector convention for displaying the amplitude and phase of the fitted harmonic, with the arrow point in the direction of the month of highest SST anomalies

The consistency of response is evaluated further using spectral analysis in order to test the coherence of SST fluctuations and the Southern Oscillation in the frequency domain in each of these sectors. The Blackman–Tukey method is utilized. Five per cent of the data are cosine-tapered on each end of the series. The analysis is based on 128 seasonal averages, utilizing a bandwidth that results in 8·9 degrees of freedom.

4. EVOLUTION OF ENSO RELATED WARM EPISODES IN THE ATLANTIC AND INDIAN OCEANS

The evolution of temperatures in the Atlantic and Indian Oceans during a composite of eight ENSO episodes is depicted in Figure 3 for the 2-year period commencing 6 months prior to the year of the onset of an ENSO episode. This includes the episodes 1951, 1953, 1957, 1963, 1965, 1968, 1972, and 1976. During the JAS (−1) and OND (−1) seasons, cold anomalies prevail in the analysis sector. Maximum cooling occurs during the OND (−1) season for the Atlantic as a whole and one season later (JFM (0)) in the Indian Ocean. In JFM of year 0, a warming begins in the south-east Atlantic, along the Benguela coast where strong upwelling occurs. This warming continues and intensifies in the AMJ (0) season. Warming commences elsewhere in the Atlantic and Indian Oceans in JAS (0) and anomalously warm conditions persist until the following year. The Atlantic as a whole reaches its peak warming around OND (0). A similar conclusion was reached by Hamilton and Allingham (1988), who found maximum warming during the 'mature' phase of ENSO toward the end of year 0. In the Indian Ocean peak warming occurs one season later, during JFM (+1). Thus, the tropical Atlantic lags the eastern Pacific by about 6 months but is roughly in phase with the central Pacific (Rasmusson and Carpenter, 1982). The western Indian Ocean lags both by an additional three months.

Concurrent wind and sea-level pressure anomalies during seasons of maximum warming and cooling in the Atlantic and Indian Oceans (Figures 4–7) indicate significant changes during the course of ENSO episodes. These are generally not large in magnitude, but tend to be opposite during warming and cooling phases, particularly over the Indian Ocean. In general, the SST, wind and pressure fields are mutually consistent and SST changes tend to be associated with wind advection of warmer or colder water.

During maximum cooling in the Atlantic, in OND (−1), the South Atlantic High is intensified and displaced eastward, while the North Atlantic High is weaker and displaced north-eastward (Figure 4). The equatorial trough is anomalously weak and displaced northward in the Atlantic and is anomalously weak in the Indian Ocean. The South Indian High appears to be intensified and displaced westward. During the season of maximum warming of the Atlantic as a whole, OND (0), the South Atlantic High is weakened and displaced westward, while the North Atlantic High is intensified and displaced south-westward. In contrast to the cooling phase, the equatorial trough appears to be anomalously strong in the Indian Ocean and anomalously strong and displaced southward in the Atlantic. The South Indian High is weakened, expanded and displaced south-westward.

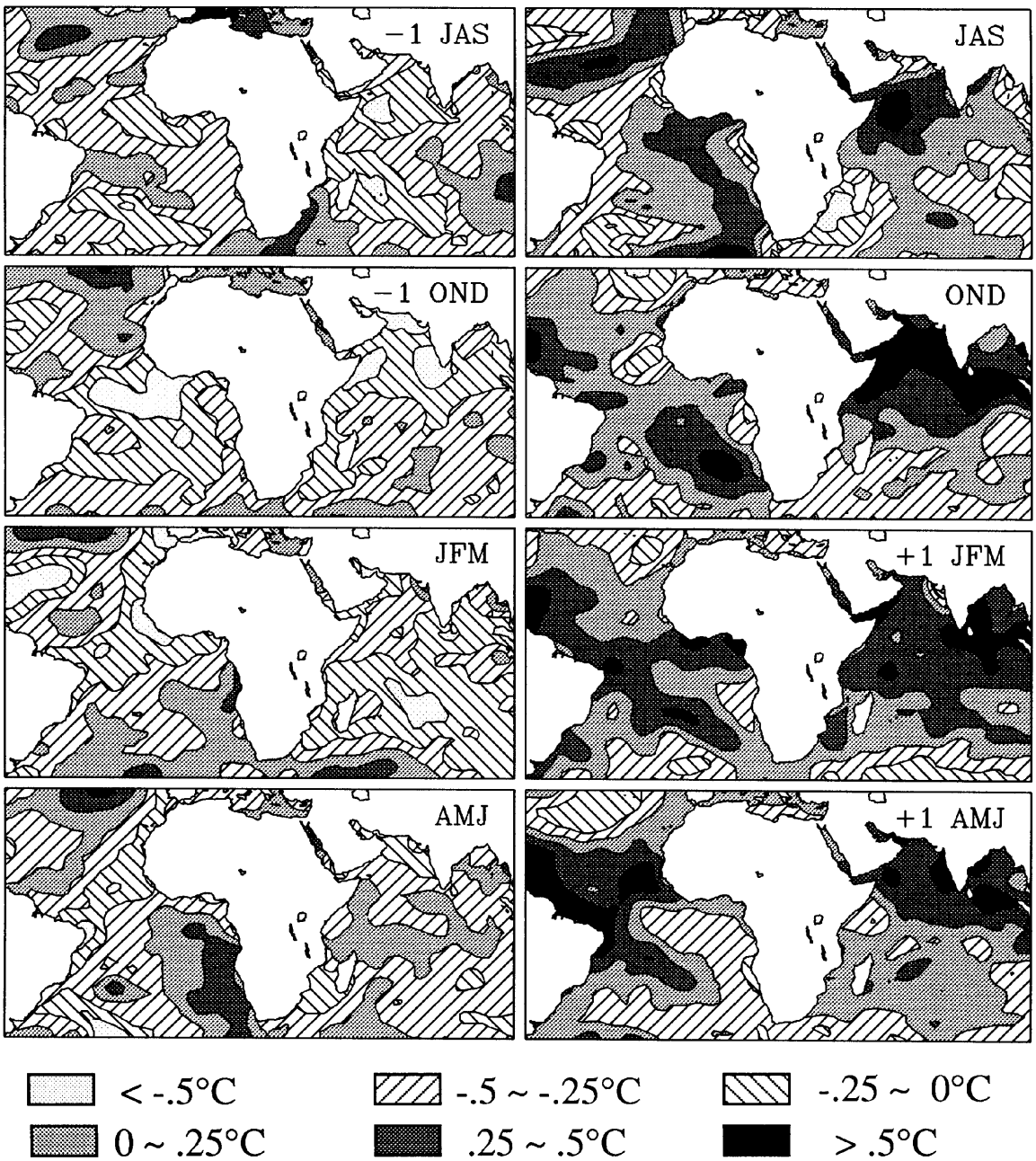

Figure 3. The SST evolution in the Atlantic and Indian Oceans during Pacific ENSO events. Composites are for 3-month seasons commencing during JAS of the year prior to ENSO. Shading represents positive anomalies, with progressively darker shading indicating anomalies of 0 to 0·25, 0·25 to 0·5, and greater than 0·5°C. Negative anomalies are indicated by right hatching (0 to 0·25), left hatching (0·25 to 0·5), and dots (greater than 0·5°C)

During the phase of maximum cooling in the Indian Ocean, JFM (0), the South Indian High is intensified and displaced south and westward (Figure 5). The equatorial trough in the Indian Ocean is intensified and displaced southward; it is weakened in the western Atlantic but is anomalously strong in the eastern Atlantic. The North Atlantic High is intensified and displaced north-westward; the South Atlantic High is weakened. During the season of maximum warming in the Indian Ocean, JFM (+1), the South Indian High is weakened and displaced north and eastward. The North Atlantic High is weakened and displaced northward, while the South Atlantic

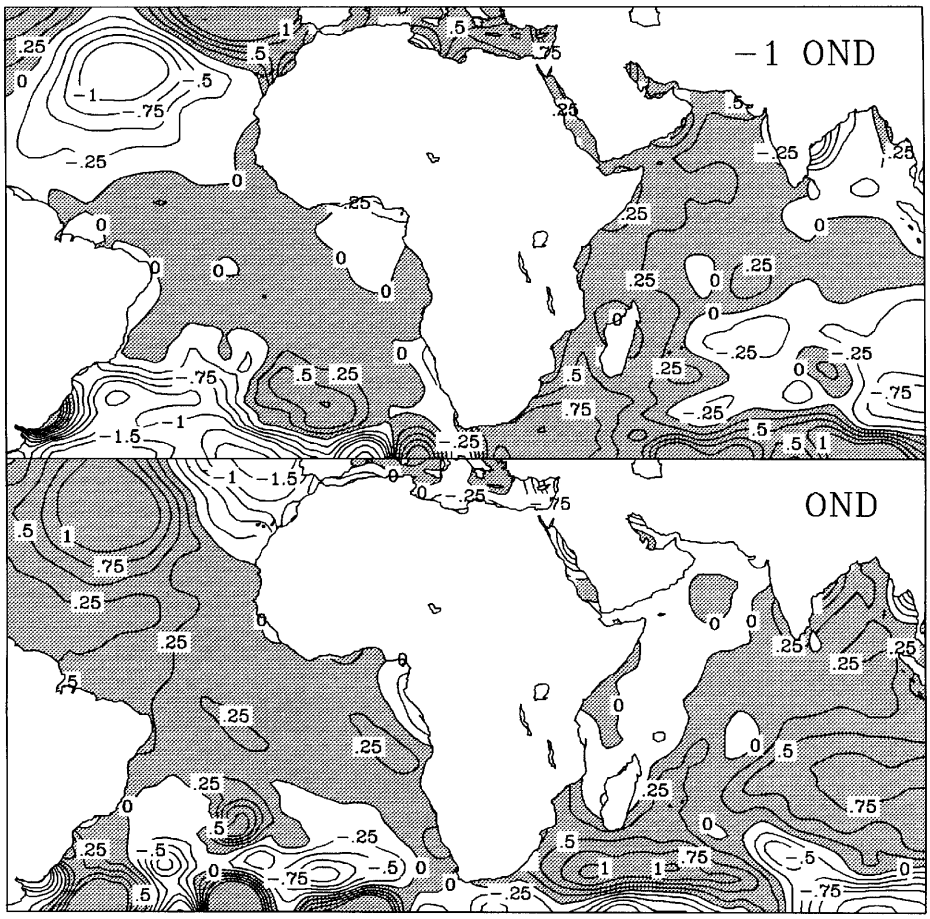

Figure 4. Composite pressure anomalies (hPa) for ENSO episodes: (top) OND of year −1, i.e. times of maximum Atlantic cooling; (bottom) OND of year 0, i.e. time of maximum Atlantic warming

High is strengthened and displaced westward. The equatorial trough in the Indian Ocean is narrowed and intensified. It is anomalously strong in the Atlantic.

The wind patterns (Figures 6 and 7) are consistent with the pressure patterns; changes in anticyclonic and cyclonic circulation and low-latitude convergence are particularly apparent. Strongest anomalies are near the North Atlantic High and in the equatorial winds and south-east trades in the Indian Ocean. Advective effects of changes in wind speed or direction can account for many of the SST changes during the ENSO cycle, but the winds are inadequate to explain all of the anomalies observed. A case in point is the negative SST anomaly in the equatorial Atlantic during OND of year 0. This may reflect the operation of remote forcing, as described in section 1 or it may also be indicative of the importance of surface heating in regulating Atlantic SSTs (Molinari *et. al.*, 1994). In view of the findings of Tourre and White (1995), that no ENSO mode is evident in near-surface heat storage in the equatorial Atlantic, the former possibility seems most likely.

5. RESULTS OF THE HARMONIC ANALYSIS

Figure 8 presents the results of the harmonic analysis performed on a composite of eight Pacific ENSO events. At the top of the figure, the magnitude and phase of the first harmonic are depicted, respectively, by the length and direction of a vector, as described in Figure 2. The strongest signals are in the south-eastern and equatorial Atlantic, in Atlantic sectors in proximity to the South American continent, and throughout most of the Indian

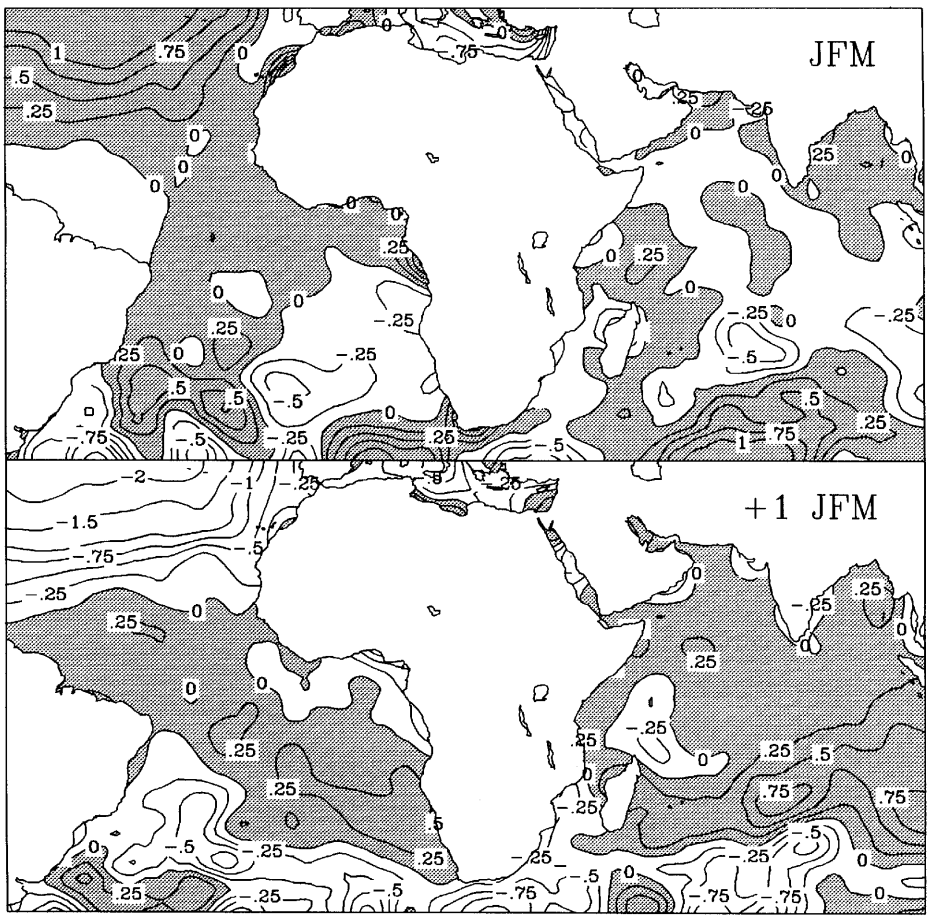

Figure 5. Composite pressure anomalies (hPa) for ENSO episodes: (top) JFM of year 0, i.e. times of maximum Indian Ocean cooling; (bottom) JFM of year +1, i.e. time of maximum Indian Ocean warming

Ocean to about 25°S and 90°E. The phase is quite diverse in the Atlantic, with warming commencing first in the south-eastern Atlantic and following several seasons later in other sectors. The phase is relatively uniform throughout the Indian Ocean, with maximum warming occurring between December of year 0 and February of the following year in most grid-squares.

From these results we have identified 10 Atlantic sectors and seven sectors in the Indian Ocean (bottom of Figure 8) in which SSTs appear to respond coherently to ENSO. In all regions, the 'coherency', as defined in section 3, far exceeds 0·9. The regions identified here are comparable with those determined by Nicholson and Nyenzi (1990) to be coherent with respect to SST fluctuations. As in Ropelewski and Halpert (e.g. 1986) these were chosen subjectively and examined further to determine if a consistent ENSO signal is evident.

The temporal evolution of SSTs in each sector during the 2-year ENSO period is shown in Figures 9 and 10. In all cases, a persistent pattern of warming and cooling is evident, with anomalies of the same sign continuing for many months and in some cases a year or more. These show that most of the Atlantic warms during the ENSO cycle and they confirm the temporal sequences shown in the composites in Figure 3. The warming begins in areas in proximity to the Benguela coast, followed by warming in the south-east Atlantic, along the Guinea Coast then off north-east Brazil. While the rest of the Atlantic warms, a sector to the west of the Canaries current cools markedly. There is also a warming trend during the ENSO cycle throughout the Indian Ocean, but, with the exception of a few sectors, the Indian Ocean clearly lags the Atlantic.

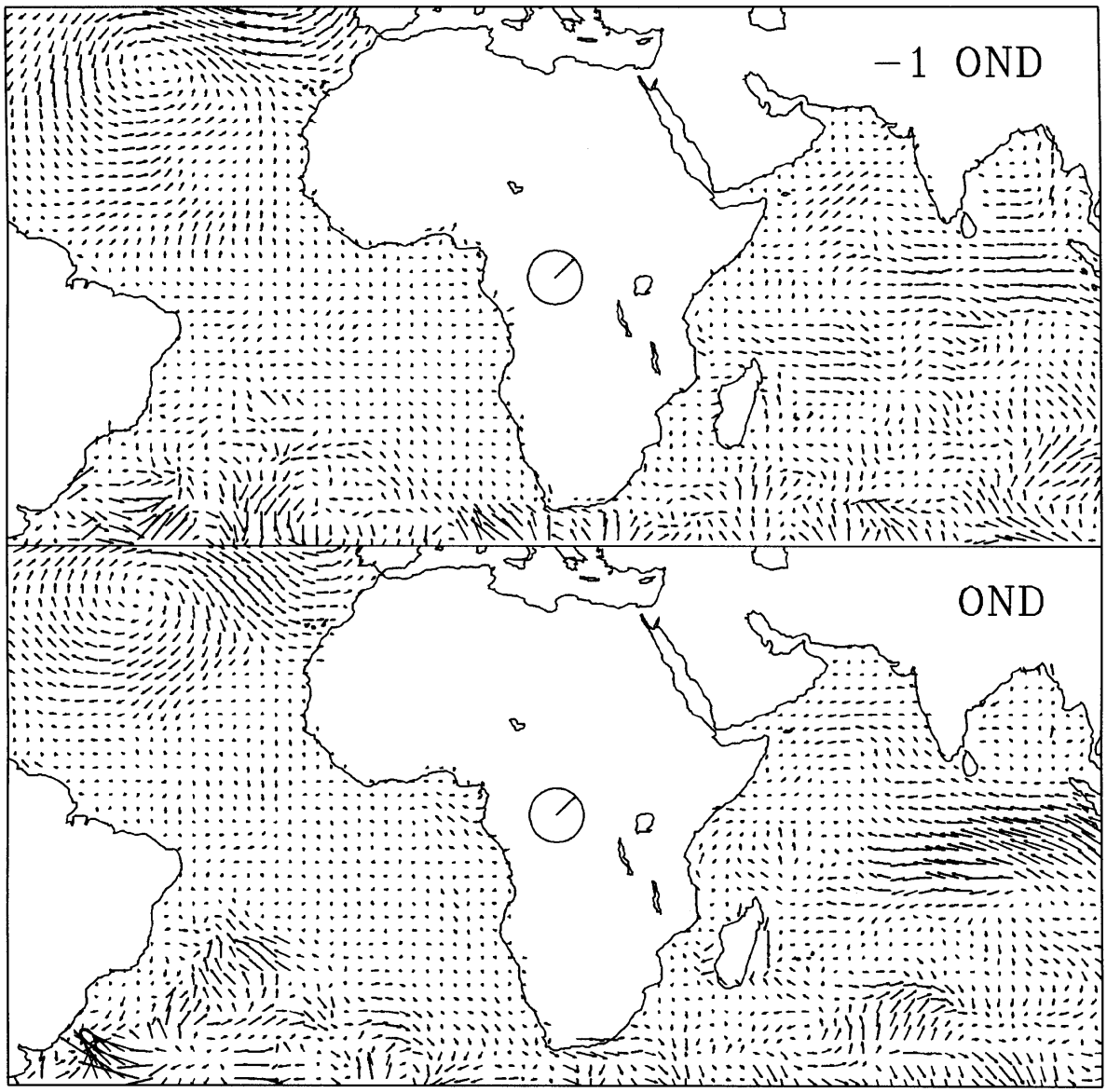

Figure 6. Composite wind anomalies for ENSO episodes. Length of circled arrow corresponds to an anomaly of 2 m s^{-1}: (top) OND of year −1, i.e. time of maximum Atlantic cooling; (bottom) OND of year 0, i.e. time of maximum Atlantic warming

Figures 9 and 10 clearly depict a cool phase in both oceans during the first half of the ENSO cycle, and a warm phase during the second half. However, an interesting contrast between the Atlantic and Indian Oceans is evident in the timing of the warming and cooling. The sectors in Figures 9 and 10 are roughly arranged from north to south. The warming begins progressively later from the south to the equatorial Atlantic (regions A9 through to A2), whereas the phase over the Indian Ocean is relatively constant. Interestingly, the northernmost sectors of the Atlantic are out-of-phase with other areas, creating a pattern reminiscent of the dipole discussed by Houghton and Tourre (1992) and others, with a node at about 10 to 15°N.

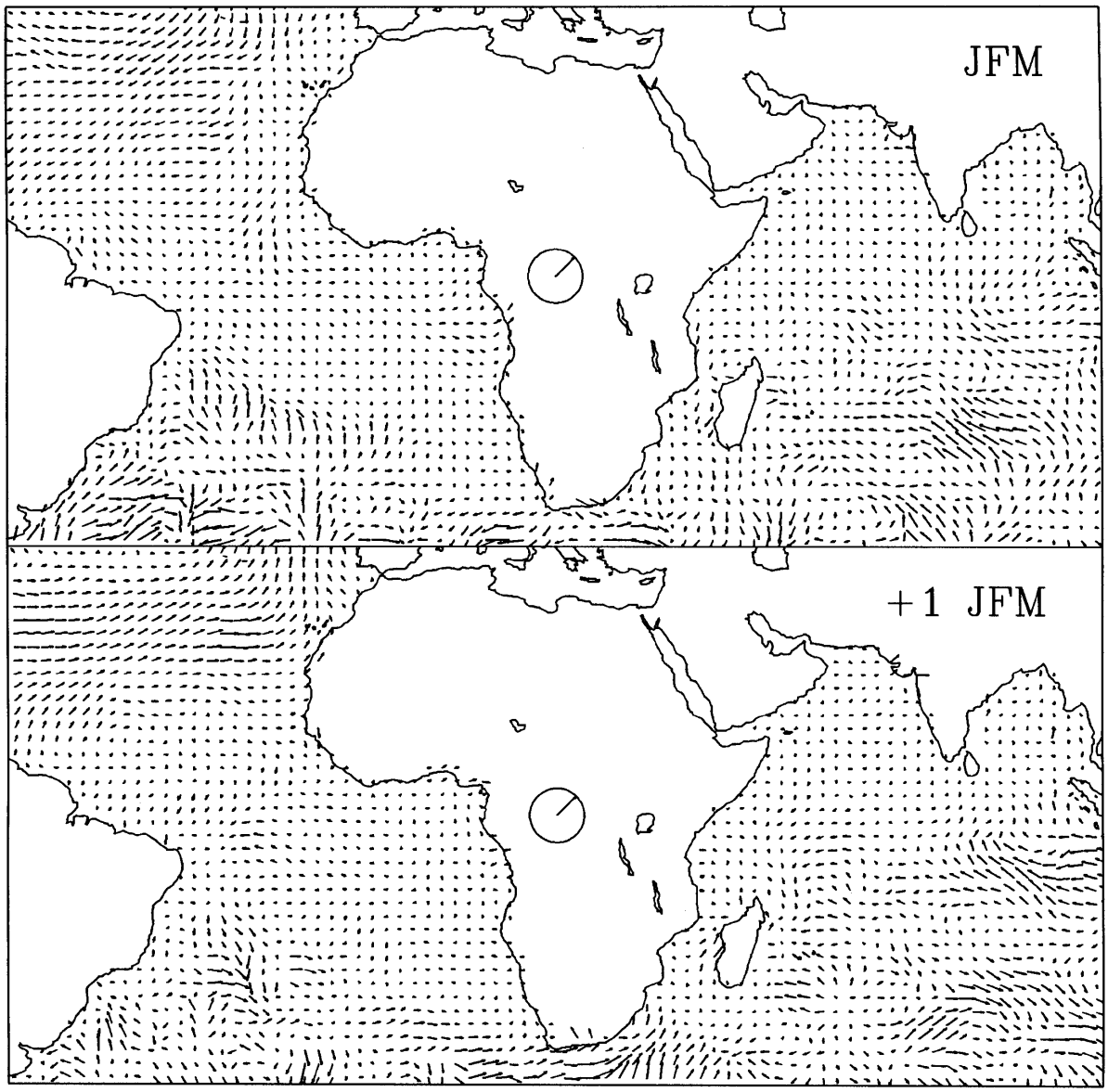

Figure 7. Composite wind anomalies for ENSO episodes. Length of circled arrow corresponds to an anomaly of 2 m s^{-1}: (top) JFM of year 0, i.e. time of maximum Indian Ocean cooling; (bottom) JFM of year +1, i.e. time of maximum Indian Ocean warming

6. CONSISTENCY OF THE ENSO SIGNAL IN THE TROPICAL ATLANTIC AND WESTERN INDIAN OCEANS

The 3-month seasons of largest negative and largest positive anomalies in the ENSO composites of Figures 9 and 10 are indicated in Table I. The SST anomaly series for each of these seasons are shown in Figures 11–14. Similar to the methodology of Ropelewski and Halpert (1987), regions are considered to have a consistent, ENSO related SST signal if the warming or cooling is evident in six out of eight ENSO episodes.

The sectors where a warming phase consistently occurs during ENSO episodes are A1, A2, A3, A4, and A5 in the Atlantic, and I1, I2, I3, I5, and I6 in the Indian Ocean. In the Atlantic, this is primarily the region where the equatorial trough is located. In the Indian Ocean, all of the sectors identified originally, except that near the East African coast, consistently show warming during ENSO episodes, generally at the end of year 0 or the beginning

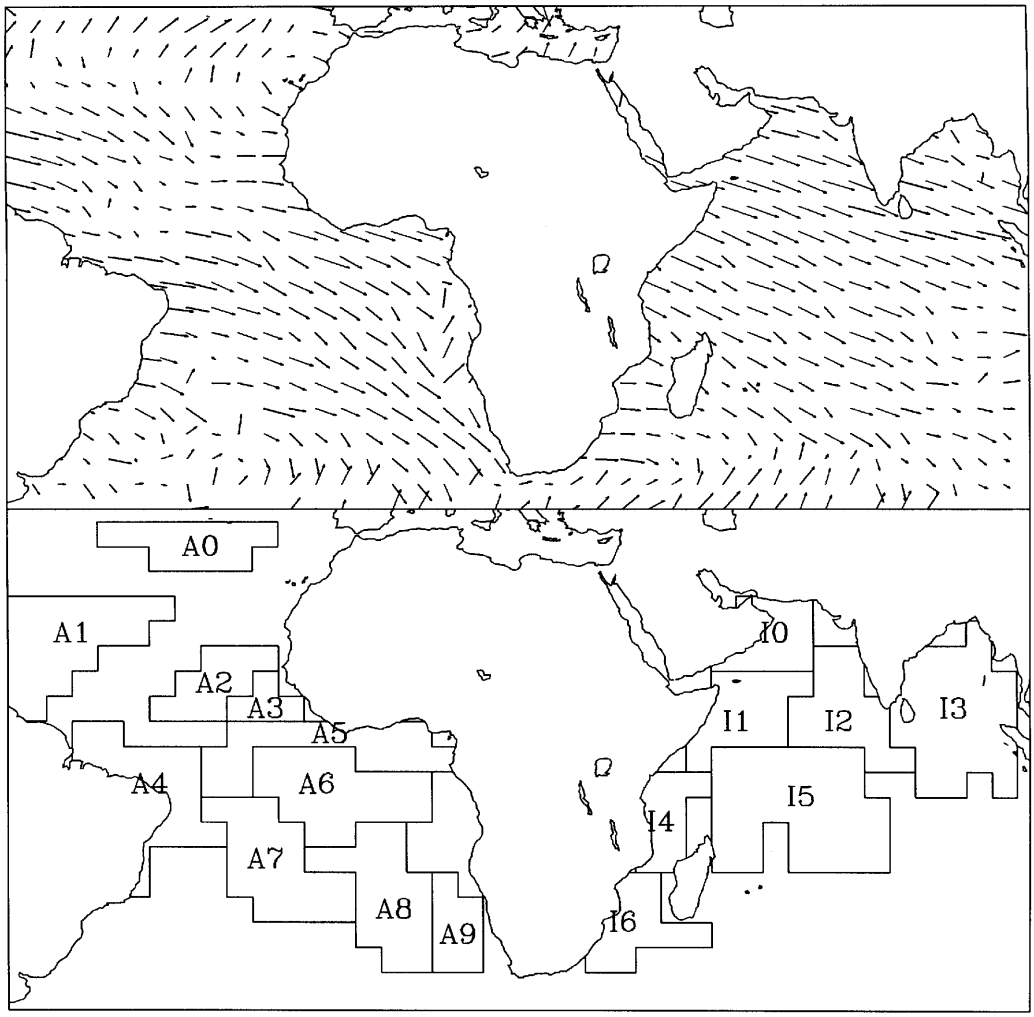

Figure 8. (Top) Results of harmonic analysis of 24-month ENSO SST composites, representing an average of eight Pacific ENSO events. See Figure 2 for interpretation of notation. (Bottom) Areas of apparent 'coherent' response which were selected for further study on the basis of the above results

of the following year. In most sectors where the ENSO warming signal does not consistently occur during the season identified, the largest positive SST anomalies are nevertheless coincident with the year of maximum warming in the Pacific (year 0) and negative anomalies almost never occur at this time during ENSO episodes. This is particularly true for sectors A6, A7, A8, A9, and I4.

Figures 15 and 16 show the full SST time series for each region in Figure 8, using seasonal averages and with ENSO years (i.e. year 0) shaded. These generally confirm the results of the harmonic analysis. They also depict the abruptness of the SST changes during ENSO events, i.e. an oscillatory behaviour characteristic of ENSO. These further indicate a clear warming in many sectors during some ENSO events, which, according to Figures 11–14, lacked a signal in the Atlantic and western Indian Oceans. One example is 1976, where abrupt warming is apparent in most Atlantic sectors. Another is 1953, when warming is evident in Figure 16 in most Indian Ocean sectors, but earlier than would be indicated by the harmonic analysis. Likewise, the 1957 warming showed up earlier than 'expected' in Atlantic sectors A7, A8, and A9, and hence it is apparent in the full time series but not in the seasonal time series of Figures 11–14.

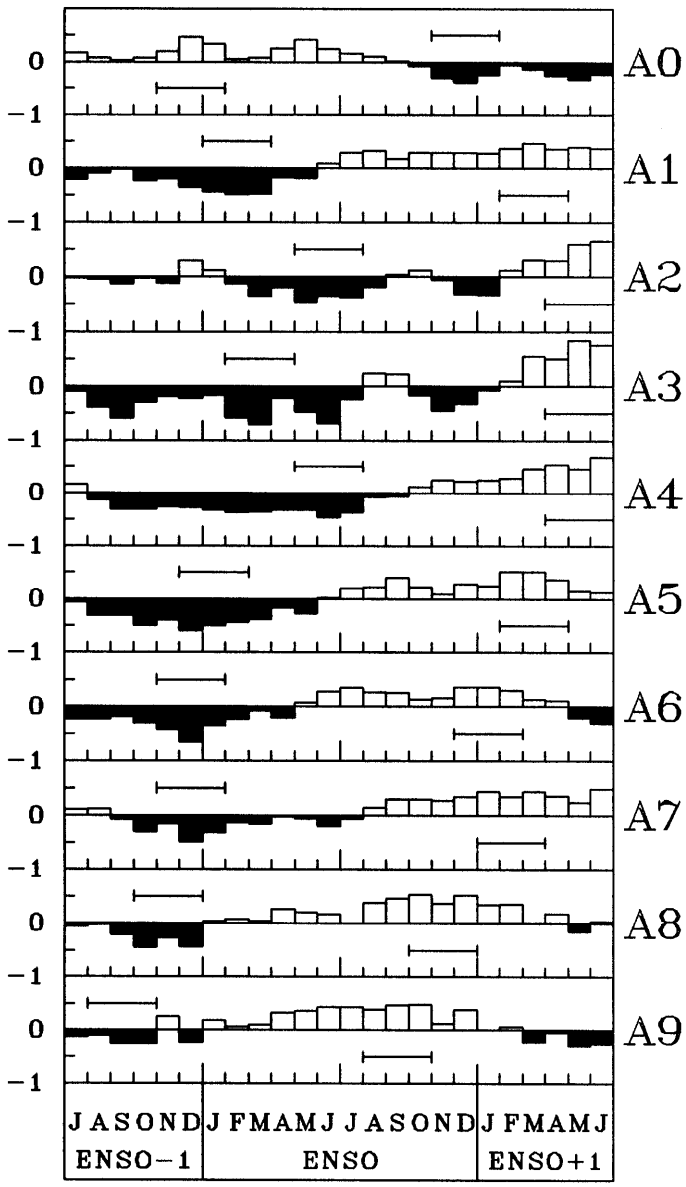

Figure 9. ENSO composite SST anomalies (standard departures) for 10 regions of the tropical Atlantic (see Figure 8). Time series commence in July in the year prior to ENSO and continue to June of the year following it. Horizontal lines indicate 'seasons' of possible ENSO related SST response, including periods of both cold and warm anomalies

These results suggest that the inconsistency in the ENSO signal is more in its timing than in its presence or absence in the Atlantic and western Indian Oceans. This was confirmed by a small modification of the analysis in which the warmest 5-month period was identified in Figure 9 and the warmest consecutive 3-month period within it during each ENSO event was plotted as in Figures 11 and 12. The warming was much more consistently apparent and its magnitude considerably greater.

Some Pacific ENSO episodes are manifested less strongly than others in the tropical Atlantic and western Indian Oceans. That of 1953 appears to have had the least impact, followed by 1976. The cool phase of the 1957 episode is evident in the Indian Ocean, but the warm phase is not. Those with the strongest and most consistent signal in both the Atlantic and Indian Oceans are 1963, 1965, 1969, and 1972. Both warming and cooling phases

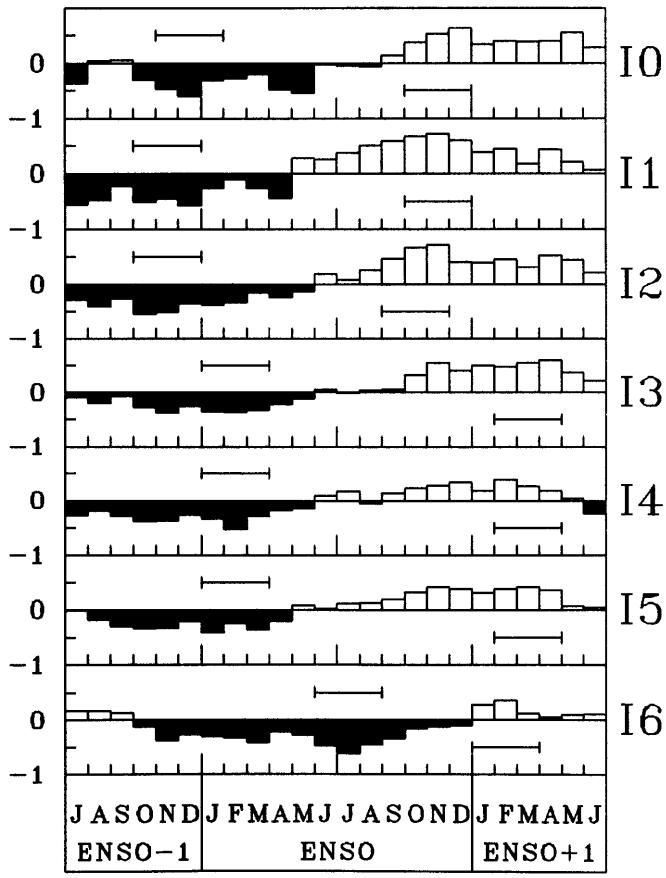

Figure 10. As in Figure 9, but seven regions of the tropical Indian Ocean (see Figure 8)

Table I. The periods of maximum warming and cooling in the Atlantic and Indian Ocean sectors of Figures 8 and 9. Indicated month is first of a 3-month period, with −1, 0, +1 signifying the years prior to, during, and after the year of the Pacific ENSO

	Warm	Cold
A0	11 (−1)	11 (0)
A1	2 (+1)	1 (0)
A2	4 (+1)	5 (0)
A3	4 (+1)	2 (0)
A4	4 (+1)	5 (0)
A5	2 (+1)	12 (−1)
A6	12 (0)	11 (−1)
A7	1 (+1)	11 (−1)
A8	10 (0)	10 (−1)
A9	8 (0)	8 (−1)
I0	10 (0)	11 (−1)
I1	10 (0)	10 (−1)
I2	9 (0)	10 (−1)
I3	2 (+1)	1 (0)
I4	2 (+1)	1 (0)
I5	2 (+1)	1 (0)
I6	1 (+1)	6 (0)

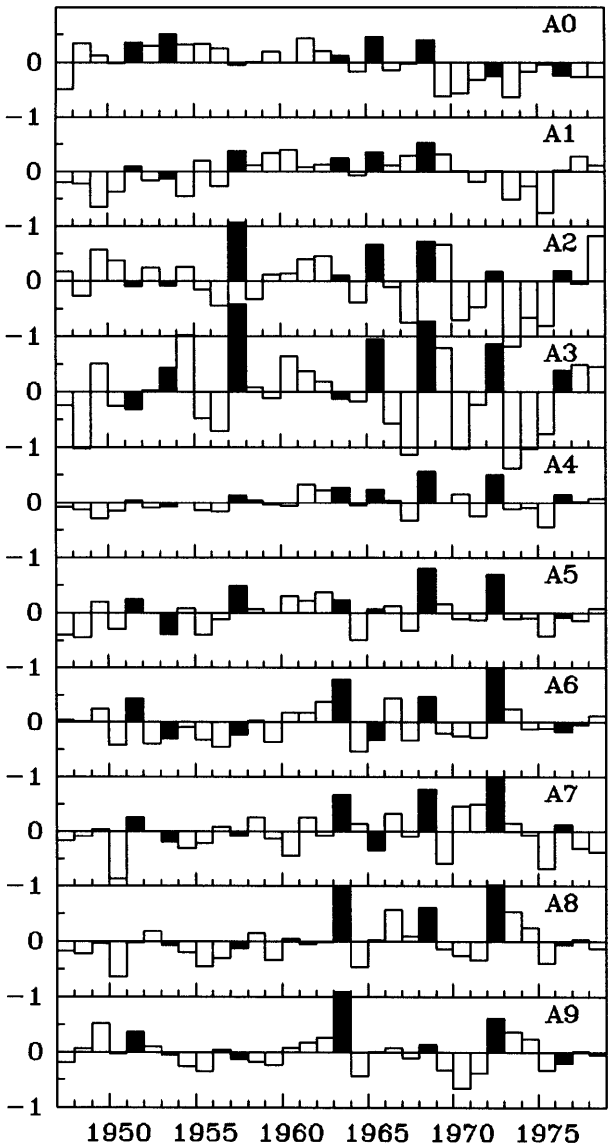

Figure 11. Time series of SST anomalies (°C) for the seasons of warm anomalies identified in Figure 9 for 10 Atlantic regions. ENSO years (i.e. year 0) are shaded

are apparent in most sectors also for the 1951 episode, but they are considerably weaker than during the episodes from 1963 to 1972.

The question arises as to the circumstances under which Pacific ENSO episodes manifest changes in the Atlantic and western Indian Oceans as well. These may relate to the characteristics of individual episodes. Schonher and Nicholson (1989), for example, found that only those events with Pacific SST anomalies persisting well into winter enhanced rainfall in California. Descriptions and classifications of Pacific events from Fu *et al.*, (1986) and Quinn *et al.*, (1978) were examined to identify any commonalities in ENSO episodes with and without strong responses in the tropical Atlantic and western Indian Ocean. No consistent differences are apparent between episodes with and without strong response in these regions (Table II).

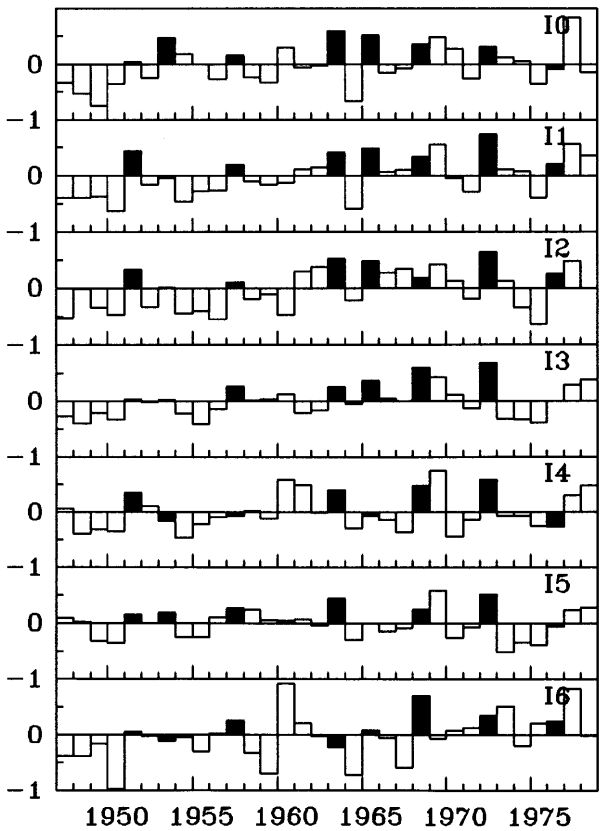

Figure 12. Time series of SST anomalies (°C) for the seasons of warm anomalies identified in Figure 10 for seven Indian Ocean regions. ENSO years (i.e. year 0) are shaded

7. COHERENCY BETWEEN SSTs AND THE SOUTHERN OSCILLATION

The Southern Oscillation shows strong quasi-periodicities of the order of 2·3, 3·5 and 4 to 6 years, with the last being dominant during the period 1935 to 1973 (Nicholson and Entekhabi, 1986). The range of 4 to 6 years is also the dominant time-scale of SST variability in the Atlantic from about 5°N to 30°S and in the western Indian Ocean from about 20°N to 10°S (Nicholson and Nyenzi, 1990). Here spectral analysis is utilized to determine the spectral coherency between SST fluctuations in the sectors shown in Figure 8 and the Southern Oscillation. The SO is represented in this analysis by the normalized series of Tahiti–Darwin station pressure differences. Seasonal (3-month) values are calculated for the analysis period, 1948 to 1979.

For the period 1948 to 1979 the SOI spectrum shows significant peaks only at about 4 to 6 and about 2 to 3 years. The latter peak attains a maximum in the quasi-biennial oscillation (QBO) range of *ca.* 2·2 to 2·4 years. The 4-to-6 year peak is evident and generally significant at or above the 95 per cent confidence level in all of the SST sectors in Figure 8 except A0 and A1 in the northern Atlantic and I0 in the south-western Indian Ocean (Figure 17(a and b)). However, even in these sectors there is significant spectral power in this range. The QBO peak is evident in all series except A3, A8, A9 and I0, but it is not always significant. A strong peak at about 10 years or longer is apparent in A0 and A1.

Figures 18 and 19 show the coherence-squared between SSTs and the SOI for these sectors. In the QBO range the coherence-squared attains the 95 per cent confidence level in all Atlantic sectors except A0, A1 and A2 and in Indian Ocean sectors I1, I2, I4 and I5. At lower frequencies there is also strong coherence between the SOI and SSTs in Atlantic sectors A2, A3, A4 and in all Indian Ocean sectors, but it tends to be greatest at about 3 to 4 years. In most of these sectors the coherence-squared remains high at 4 years and longer.

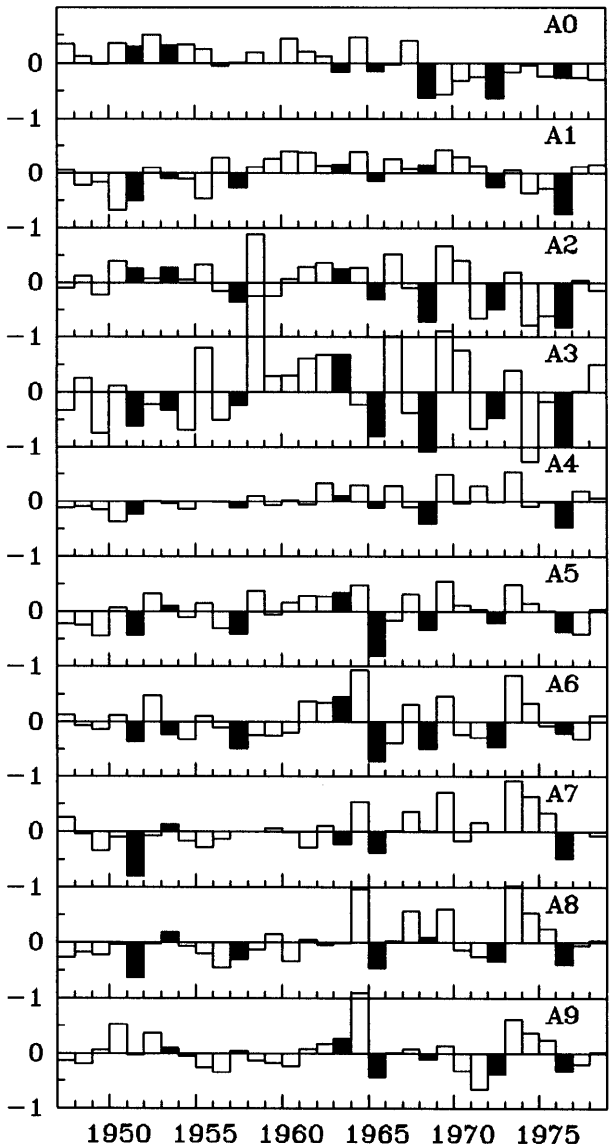

Figure 13. Time series of SST anomalies (°C) for the seasons of cold anomalies identified in Figure 9 for 10 Atlantic regions. ENSO years (i.e. year 0) are shaded

These results are consistent with the conclusions of the harmonic analysis, but they indicate a more consistent ENSO signal in sectors A6 to A9 than suggested by the time series in Figures 11 and 13. In general, the coherence with the SOI is much stronger for the Indian Ocean than for the Atlantic; it is also evident in a broader spectral band in the Indian Ocean. This suggests a stronger and more consistent ENSO signal in the Indian Ocean than in the Atlantic, a result also consistent with the conclusions of the harmonic analysis. Weakest coherence is with the northernmost Atlantic sectors (A0 and A1).

The weak coherence in sector A0 is interesting in view of the apparent out-of-phase relationship (Figure 9) between this sector and those south of about 10°N. This pattern is consistent with the dipole evidenced by Semazzi *et al.*(1988) and others and strongly resembles the first principal component in Houghton and Tourre's (1992) analysis of Atlantic SSTs. Houghton and Tourre argue that this pattern of opposite anomalies does not arise from temporally coherent out-of-phase fluctuations and is hence not a true dipole. The spectral contrast

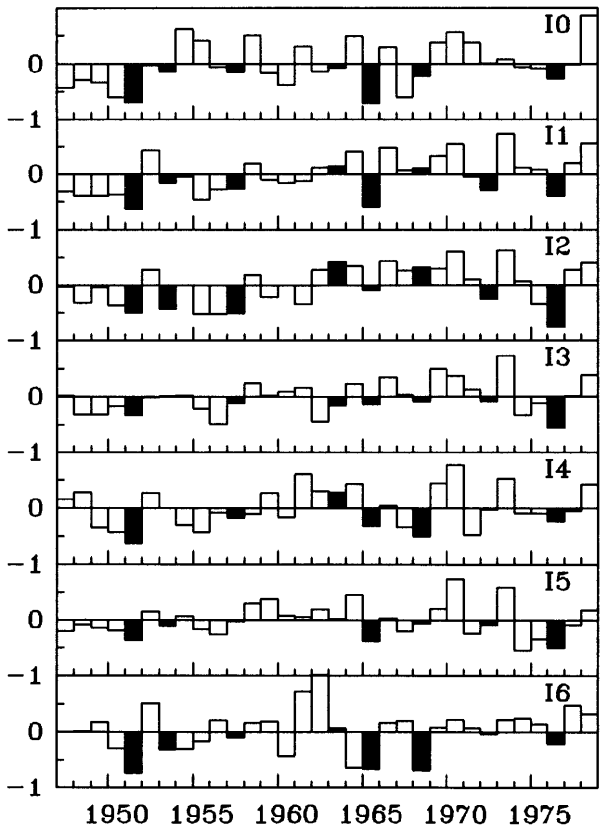

Figure 14. Time series of SST anomalaies (°C) for the seaons of cold anomalies identified in Figure 10 for seven Indian Ocean regions. ENSO years (i.e. year 0) are shaded

between sector A0 and sectors south of the apparent node near 10°N and the lack of coherence of SSTs in A0 with the SOI support this conclusion. This sector, situated north of the ITCZ, has a strong spectral peak at about 10 years, comparable to that of the North Atlantic Oscillation (Deser and Blackmon, 1993). The pattern of SST, pressure and wind anomalies resembles that of the North Atlantic Oscillation. Thus, SST variability in sector A0 may be linked to ENSO via the North Atlantic Oscillation.

8. THE 1982–1983 and 1986–1988 ENSO EPISODES

Both the 1982–1983 ENSO episode and the ENSO cycle of 1986–1989 were unusual compared with previous episodes. During the 1982–1983 episode, the timing and duration of the South American warm SST anomaly contrasted strongly with previous events. The warming began late in 1982 and peaked in December; after a brief cooling, SSTs again peaked in June 1983, well after the peak warming in the central Pacific. This is counter to the usual course of ENSO episodes (Rasmusson and Carpenter, 1982), during which warming along the South American coast peaks early in year 0, well before the anomaly in the central Pacific. The 1982–1983 episode was also unusually intense. The 1986–1988 episode was unusual both in timing and duration, with warm anomalies not appearing until mid-1986 but continuing throughout 1987 (Rasmusson and Mo, 1993).

Because of these unusual characteristics, a typical course of development in the Atlantic and Indian Oceans is not to be expected. However, the comparison with earlier episodes shows some interesting contrasts. In this case, because of the climatic shift to warmer conditions during the mid-1970s (Graham, 1994), SST anomalies are calculated with respect to the 1979–1990 mean.

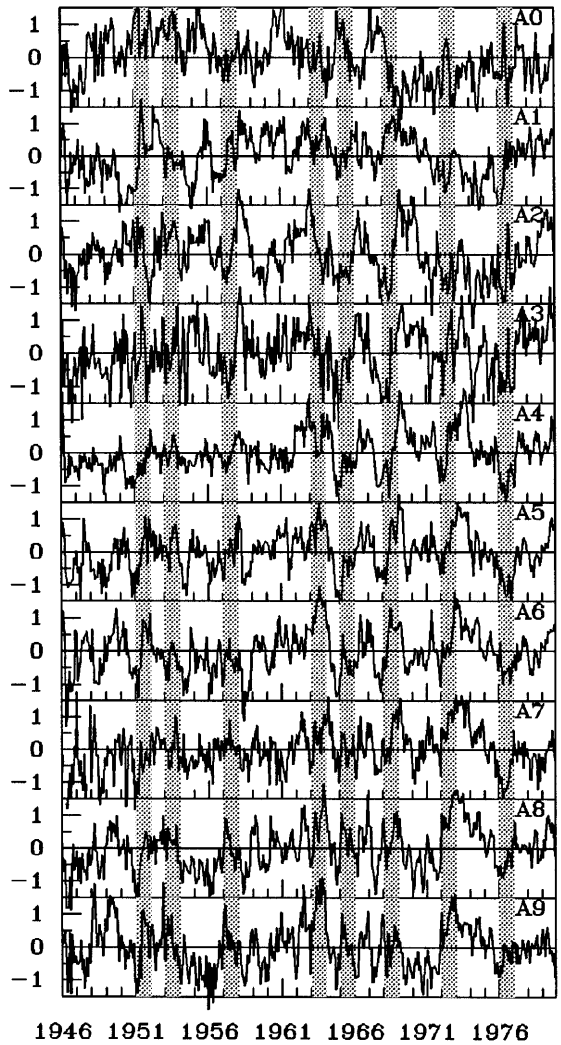

Figure 15. Time series of SST anomalies (3-month averages) for Atlantic Ocean sectors, 1946 to 1979, with ENSO years (year 0) shaded

The evolution of SSTs in the Atlantic and Indian Oceans during the 1982–1983 event (Figure 20(a)) clearly shows the development of a warm episode. Its phase in the Indian Ocean is that shown by the eight-episode composite (Figure 3), but in the Atlantic its phase is shifted 6 to 9 months later and two peaks are apparent, in JFM ($+1$) and JFM ($+2$). Interestingly, the SST anomaly along the South American coast evolved in a manner quite similar to the Atlantic, but leading the Atlantic by 6 to 9 months, as in other episodes of the composite. As with Indian Ocean SSTs, the SST evolution in the central Pacific during 1982–1983 was not unusual, paralleling the six-episode composite of Rasmusson and Carpenter (1982). This raises the intriguing possibility of independent ENSO modes in the Atlantic and Indian Oceans, with the Atlantic showing strong teleconnections to the South American coastal sectors of the Pacific and the Indian Ocean showing strong teleconnections to the central Pacific.

During the 1986–1988 episode, the unusual timing and duration of the Pacific episode, evident throughout the Pacific, have their parallel in SSTs in the Atlantic and Indian Oceans. The onset in the Pacific was 6 to 9 months later than usual and the episode lasted several seasons longer. This is quite apparent in both the tropical Atlantic and western Indian Oceans Figure 20(b)).

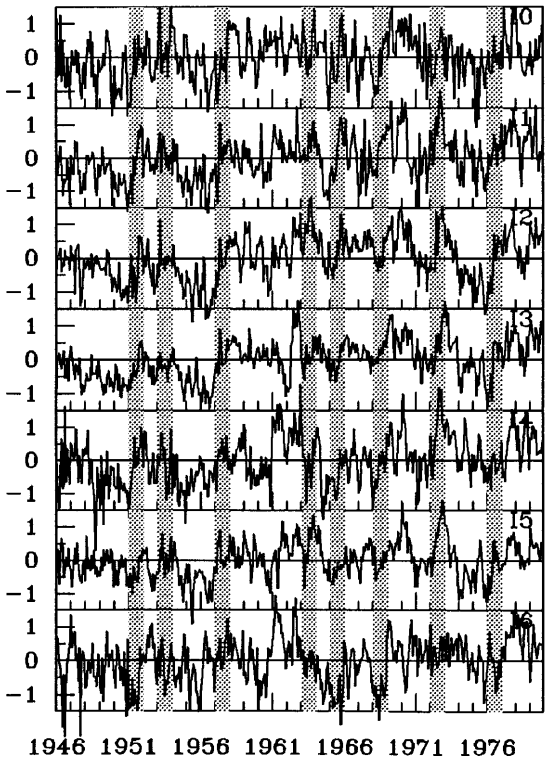

Figure 16. Time series of SST anomalies (3-month averages) for Indian Ocean sectors, 1946 to 1979, with ENSO years (year 0) shaded

9. THE QBO SIGNAL IN THE ENSO RESPONSE IN THE TROPICAL ATLANTIC AND INDIAN OCEANS

A number of authors have suggested that a quasi-biennial oscillation is an integral component of ENSO and that ENSO may be an amplification of the biennial cycle (e.g. Meehl, 1987, 1993; Lau and Sheu, 1988; Rasmusson *et al*, 1990). The biennial oscillation is dependent on air–sea interaction and simple models have shown that biennial signals could arise from an interactive ocean–atmosphere system (Brier, 1978; Nicholls, 1978, 1979, 1984; Lau and Sheu, 1988). Others have suggested that the biennial oscillation itself represents an amplification/deamplification of the annual cycle (Gutzler and Harrison, 1987; Meehl, 1987, 1993; Lau and Sheu, 1988).

Table II. Classification of ENSO episodes according to impact in the Atlantic and Indian Oceans and according to works of Fu *et al.* (1986) and Quinn *et al.* (1978). See Schonher and Nicholson (1989) for details.

Atlantic/Indian	Year	Fu *et al.*	Quinn *et al.*
No impact	53	2	—
Inconsistent or	51	1	Weak
weak impact	57	1	Strong
	65	1	Moderate
	76	3	Moderate
Strong impact	63	2	Very Weak
	68	1	—
	72	1	Strong

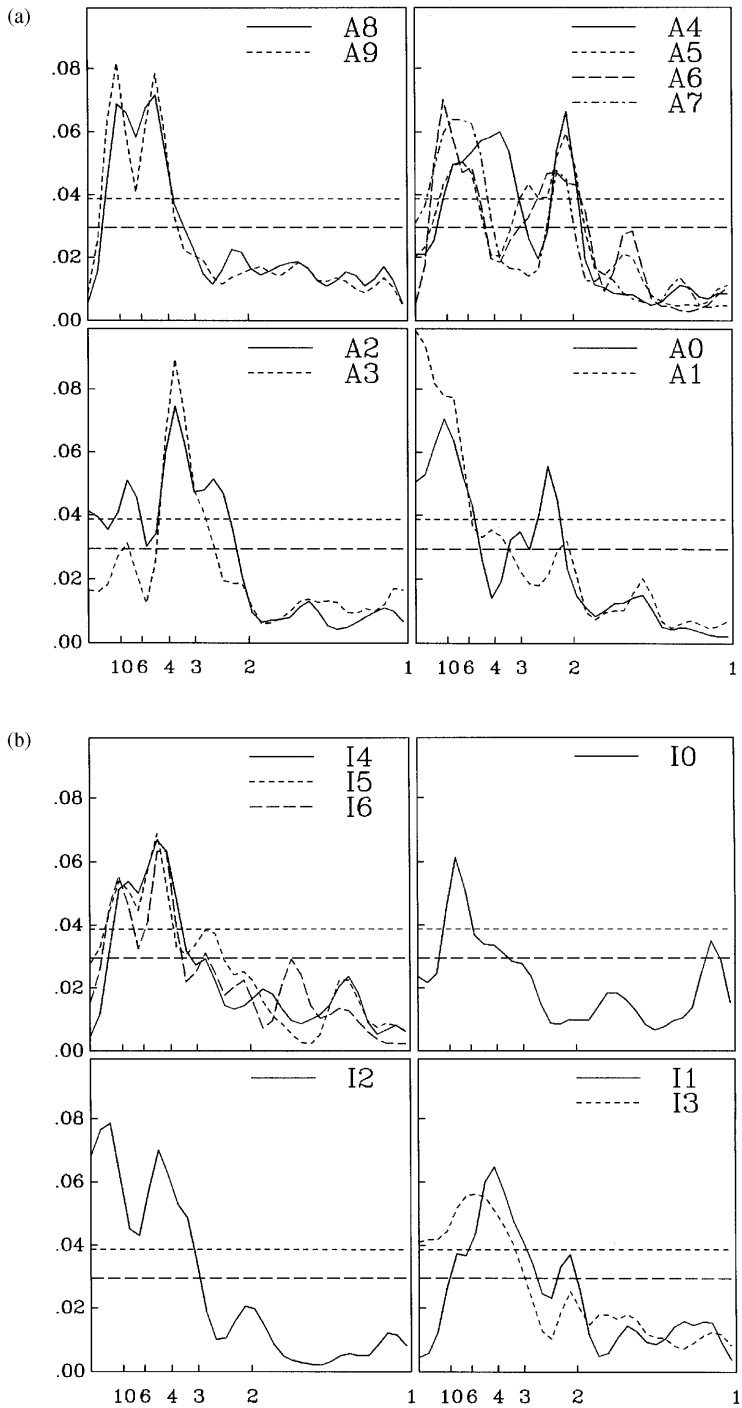

Figure 17 (a) Spectra of SSTs in the Atlantic regions illustrated in Figure 8. Sectors with spectra having common characteristics are grouped. (b) As in (a) but for SSTs in the Indian Ocean regions illustrated in Figure 8. The horizontal lines indicate 99 and 95 per cent confidence levels

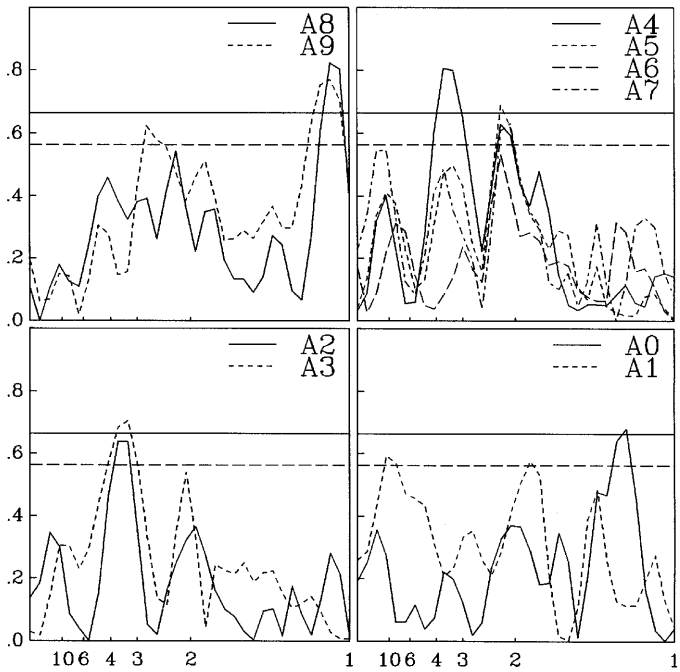

Figure 18. Coherence-squared between the Southern Oscillation Index and Atlantic SSTs for sectors in Figure 8. 99 and 95 per cent confidence levels given by solid and dashed lines, respectively

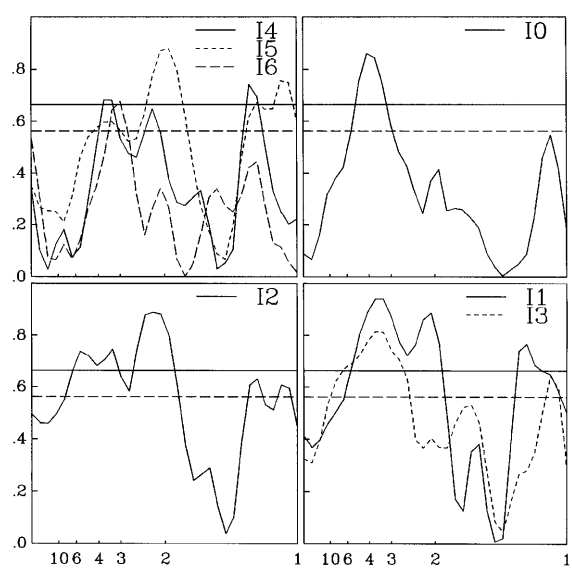

Figure 19. Coherence-squared between the Southern Oscillation Index and Indian Ocean SSTs for selected sectors from Figure 8. 99 and 95 per cent confidence levels given by solid and dashed lines, respectively

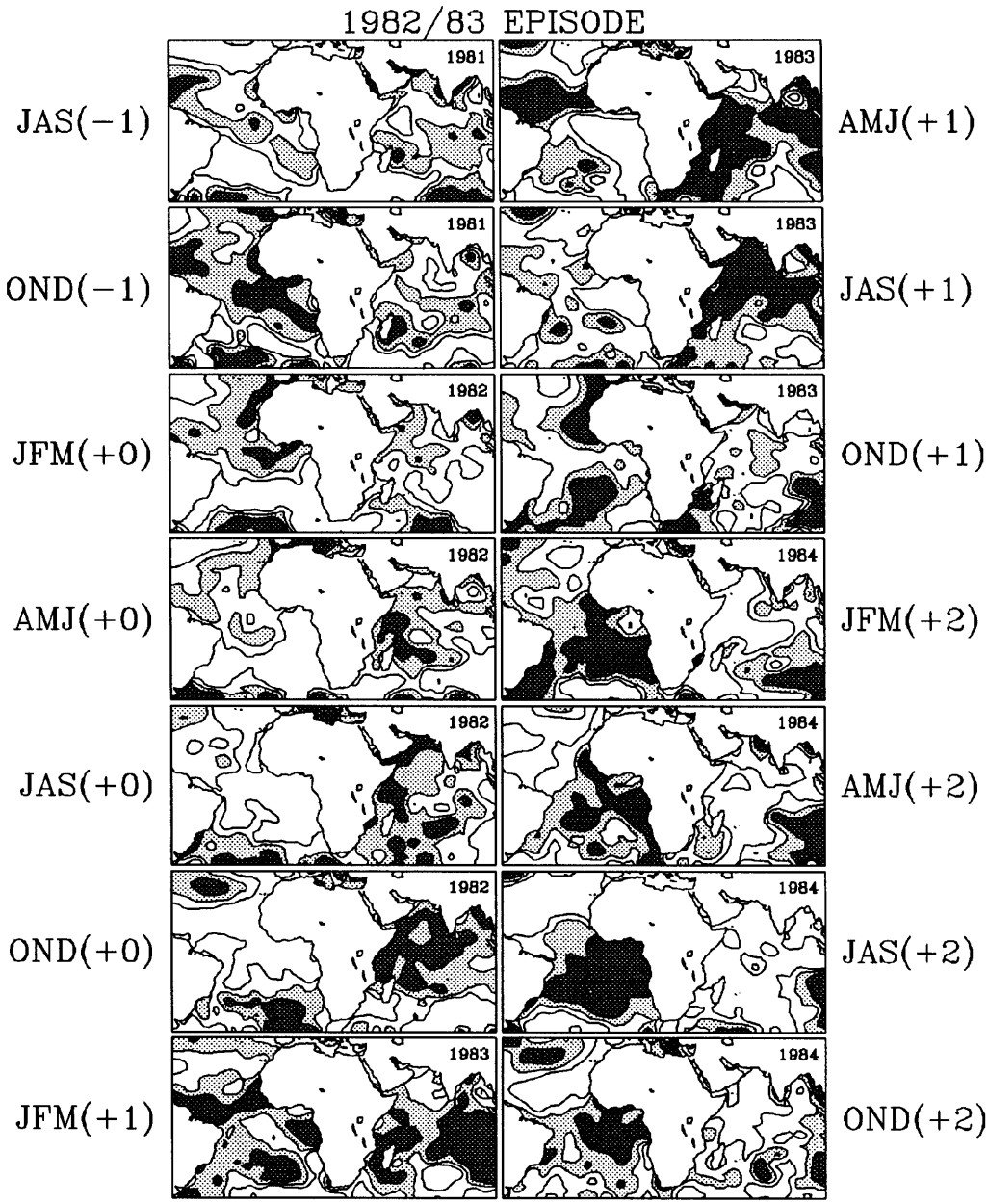

Figure 20. (a) SST evolution in the Atlantic and Indian Oceans during the 1982–83 Pacific ENSO event. Composites are for 3-month seasons commencing during JAS of year −1. Units are °C. The episode extends from July 1981 to June 1984. Light shading indicates positive anomalies less than 0·25°C; darker shading indicates positive anomalies exceeding 0·°C. Unshaded areas indicate negative anomalies, with an isopleth at −0·25°C

Meehl (1987, 1993) has described the biennial cycle in the tropical Indian and Pacific Oceans and proposes dynamic processes involving atmosphere–ocean coupling and variations in upper ocean heat content as the mechanism producing it. A comparison of the results of the current paper with those of Meehl is interesting, as it reaffirms many of his conclusions.

Meehl demonstrates (1987) that the opposite patterns of SSTs, sea-level pressure (SLP) and wind prevail during years of strong and weak monsoons over India, which are also years of strong and weak annual cycles

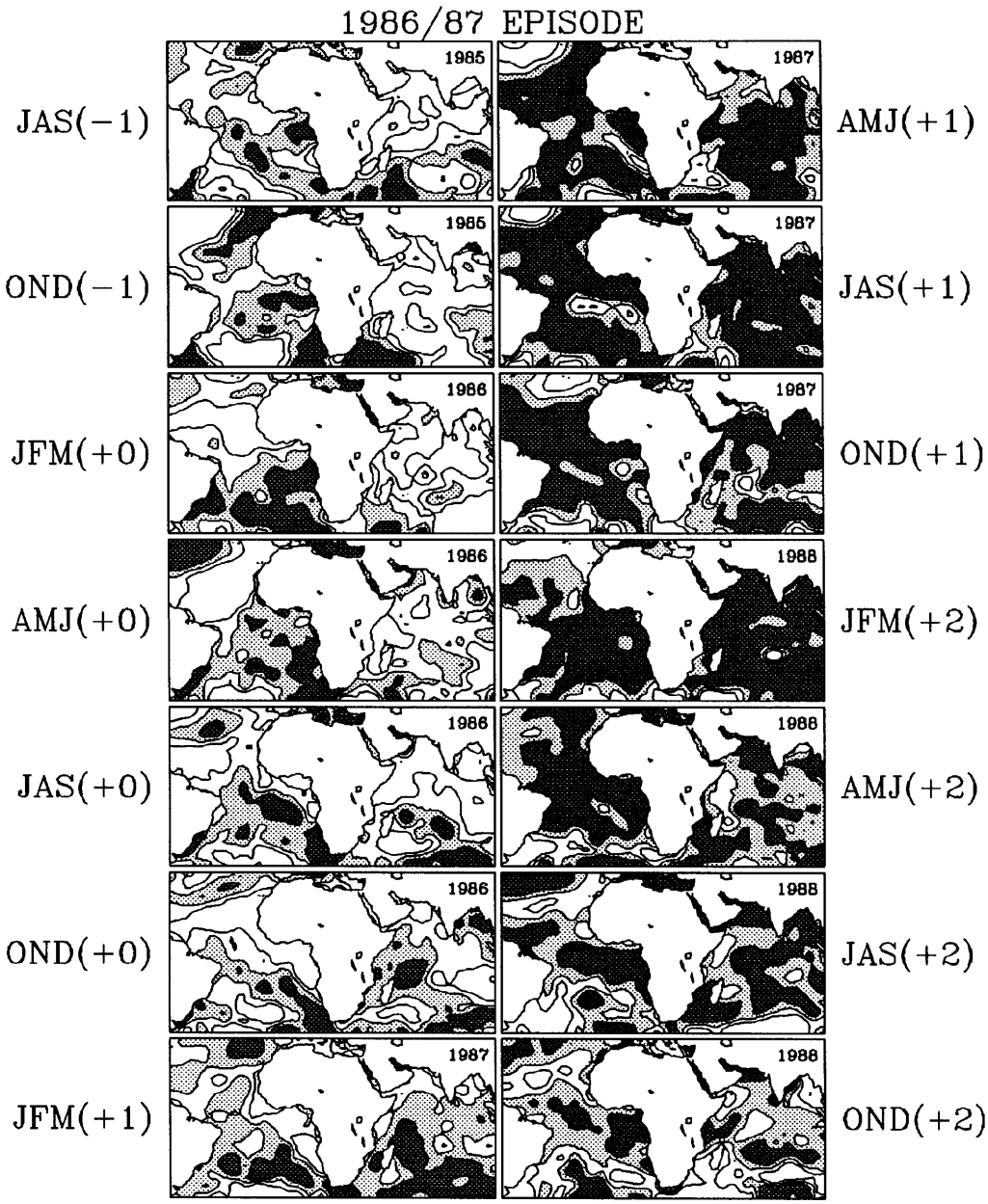

Figure 20. (b) SST evolution in the Atlantic and Indian Oceans during the 1986–88 Pacific ENSO event. The episode extends from July 1986 to June 1989. Otherwise as in (a)

respectively. These years tend to occur as couplets, producing a biennial cycle; they also tend to coincide with Cold and Warm events, respectively, as defined by van Loon (1984) or van Loon and Shea (1985), for example. The composite anomalies for these Cold and Warm events (equivalent to ENSO events) are complementary and strikingly similar to, but of greater magnitude than, those of strong and weak monsoons/annual cycles.

The SST and sea-level pressure patterns evident in the cold and warm phases of the Atlantic and Indian Oceans strongly resemble those for Meehl's strong and weak phases, respectively (Figures 3 and 21). There is some indication in the SST and pressure fields that the annual cycle is intensified during the cold phase and weakened during the warm phase, consistent with Meehl's findings for the Indian and Pacific Oceans. This is consistent with

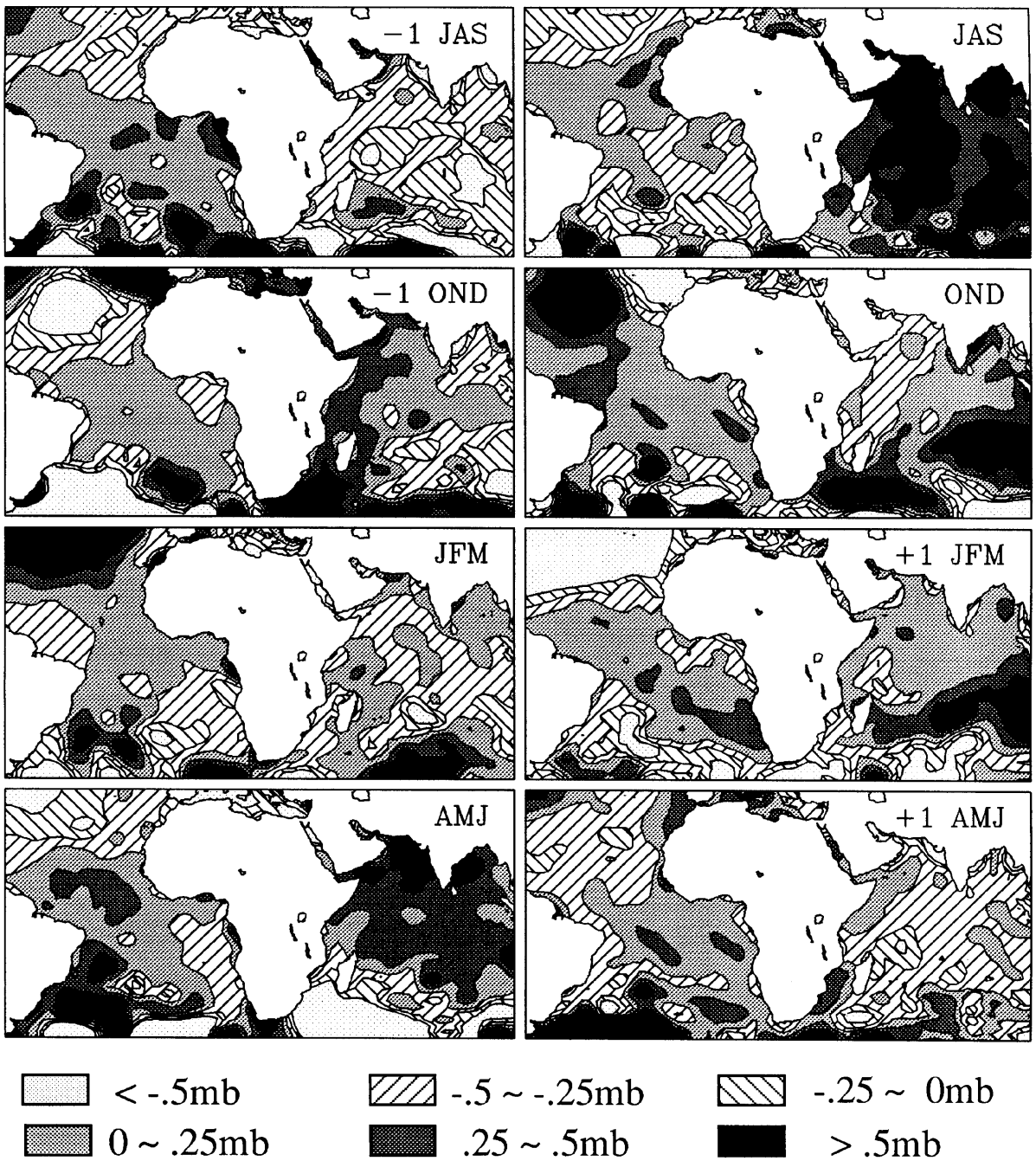

Figure 21. Sea-level pressure evolution in the Atlantic and Indian Oceans during Pacific ENSO events. Composites are for 3-month seasons commencing during JAS of year −1. Shading represents positive anomalies, with progressively darker shading indicating anomalies of 0 to 0·25, 0·25 to 0·5 and greater than 0·5 hPa. Negative anomalies are indicated by right hatching (0 to 0·25), left hatching (0·25 to 0·5), and dots (greater than 0·5 hPa)

Hastenrath's (1984) conclusion that interannual variability in the tropical Atlantic sector is manifested mainly as a weakening or intensification of the annual cycle. The quasi-biennial nature of the cold and warm phases in this region is also clearly shown by the striking reversal of SST, wind and pressure anomalies. This is apparent in all seasons in SSTs (Figure 3) and to lesser extent in sea-level pressure (Figure 21). The reversal is particularly strong during the seasons of maximum cooling or warming in the two oceans (Figures 4–7). Furthermore, strong QBO peaks are apparent in SST spectra, especially for Atlantic sectors (Figure 17) and for the dominant mode of SST variability in both oceans (Nicholson and Nyenzi, 1990).

The mechanism proposed by Meehl (1987, 1993) involves the modulation of the annual cycle of convection by way of the effect of convection on the heat content of the upper ocean. Strong convection intensifies low-level winds, promoting heat loss, mixing and, ultimately, lower SSTs and reduced heat content following the season of convective activity. Assuming the so-produced anomalies persist until the following year, convective activity 1 year later would be relatively weak, creating a biennial cycle in the system. The results of the current study clearly show the multiseason persistence SST anomalies and the sequence of changes predicted by Meehl.

The association between pressure and SST fields in the Indian Ocean (Figures 3 and 21), which suggests the importance of the surface heat balance in temperature fluctuations, is likewise consistent with this idea. The warming begins in AMJ of year 0, at a time when strong positive anomalies in sea-level pressure abruptly develop throughout most of the Indian Ocean. Warming continues through the next three seasons, during which time pressure anomalies remain positive. Cooling commences in AMJ of the year following ENSO, coincident with a switch to negative pressure anomalies over the Indian Ocean. The relationship is less clear in the Atlantic, where advection can explain most of the evolution of SST anomalies during the course of the 2-year ENSO cycle.

10. COLD AND WARM PHASES AND ASSOCIATIONS WITH AFRICAN RAINFALL

The first half of the ENSO cycle corresponds to a cold phase in the tropical Atlantic and western Indian Oceans, the second half of the cycle to a warm phase in these regions (Figures 3, 9, and 10). Rainfall anomalies over the African continent likewise reverse during these two phases. Except for the OND season, the cold and warm phases correspond roughly to 'wet' and 'dry' phases (Figure 22), respectively, over Africa (Nicholson and Kim, 1996). The timing of SST changes during these phases is quite different for the two oceans. Also the consistency of the appearance of the ENSO signal is different for these two phases. These characteristics can help to assess the role of these oceans in modulating African rainfall.

A marked difference between the Atlantic and Indian Oceans is apparent in the timing of warming and cooling. As noted in section 5, there is a clear 'propagation' of the ENSO signal northward from the south to equatorial Atlantic during both phases, with the onset and maxima of warming and cooling occurring progressively later further north. In contrast, the appearance of warm and cold anomalies is roughly in phase throughout most of the Indian Ocean. A diagram similar to Figures 9 and 10, but showing composited monthly rainfall anomalies during the 2-year course of ENSO episodes (Figure 23), provides an interesting comparison. The northward propagation of the signal from southern to equatorial Africa is strongly apparent during the cold phase and it is synchronous in timing and latitude with the propagation of the SST signal in the Atlantic. The timing of the rainfall anomalies is comparatively consistent during the warm phase. This may indicate that the control of rainfall over southern and equatorial Africa switches from the Atlantic during the cold phase to the Indian Ocean during the warm phase. However, the largest rainfall anomalies tend to occur between February and May of year 0 throughout most of the continent (Nicholson and Kim, 1996), the period of maximum warming the Atlantic.

Figure 24 shows the consistency with which anomalies of the appropriate sign appear during the appropriate season of the warm and cold phases, as in Table I. Those for rainfall are derived from the study of Nicholson and Kim and are based on all episodes since 1901. Two generalizations are clearly apparent: in the Atlantic the ENSO 'response ' appears with greater consistency during the cold phase than during the warm phase and in the Indian Ocean the warm phase ENSO 'response' appears more consistently than the cold phase 'response'. Over equatorial and Southern Africa, the rainfall response to ENSO appears more consistently in the warm phase than during the cold phase. This association may likewise suggest that the Indian Ocean tends to control rainfall anomalies during the warm phase.

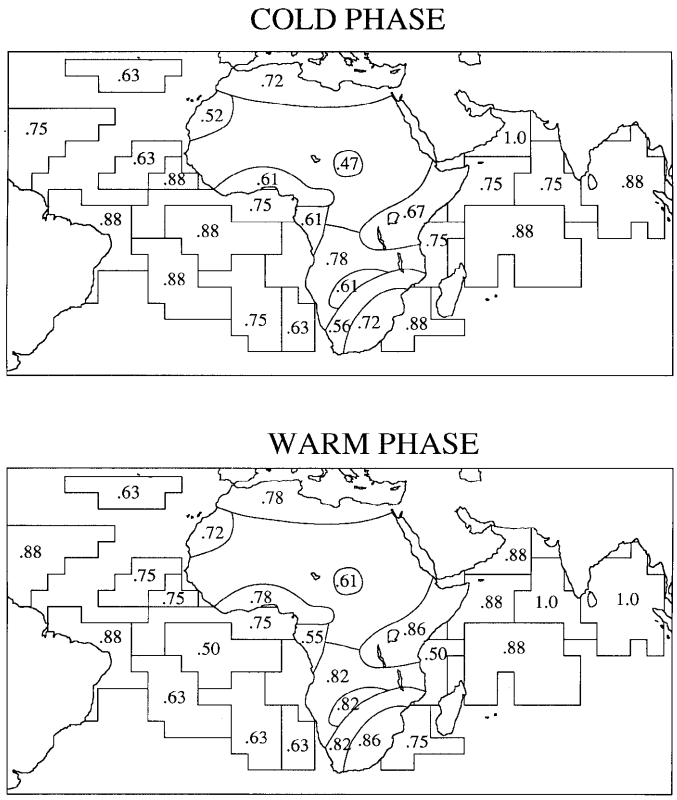

Figure 22. The consistency of the ENSO response in SSTs and rainfall during the 'cold phase' (July (−1) to June (0)) and during the 'warm phase' (July (0) to June (+1). For SSTs, the numbers indicate the percentage of ENSO episodes in which anomalies of the appropriate sign appear during the 'expected' season, as indicated in Table I. For rainfall, the value has a comparable meaning, but is based on all episodes since 1901 and is derived from Nicholson and Kim (1996)

It is interesting to note that the ENSO episode with the weakest response in rainfall (1976–1977) also has the weakest signal in the tropical Atlantic and western Indian Oceans. This might imply that rainfall is modulated directly by the ocean sectors in proximity to the African continent, with the apparent ENSO signal in rainfall being a manifestation of ENSO's influence on the Atlantic and Indian Oceans. This conclusion is supported by earlier work of Nicholson and Entekhabi (1987), who showed that throughout equatorial and southern Africa rainfall varies more coherently with Atlantic SSTs than with the SOI.

11. SUMMARY AND CONCLUSIONS

Large areas of the tropical Atlantic and western Indian Oceans are shown by harmonic analysis to consistently exhibit interannual SST variations linked to the Pacific ENSO. These areas include the seven regions in the Indian Ocean and six of the ten Atlantic regions depicted in Figure 8. The remaining four Atlantic sectors (A6, A7, A8, and A9 in the South Atlantic) have warming and cooling phases in the seasons identified during four or five of the eight ENSO episodes analysed; in the remaining episodes, a pronounced warming generally occurs but its timing differs from that suggested by the harmonic analysis. In general, these are the areas where, during the ENSO composite, warming first occurs; this is usually early in year 0 when cold anomalies prevail over most of the Atlantic.

During the first half of the ENSO cycle (i.e. July (− 1) to June (0)) a cold phase tends to occur in the tropical Atlantic and western Indian Ocean, a warm phase during the second half of the cycle. Warming in these ocean regions tends to lag the eastern Pacific by 6 to 9 months but is roughly in phase with the central Pacific.

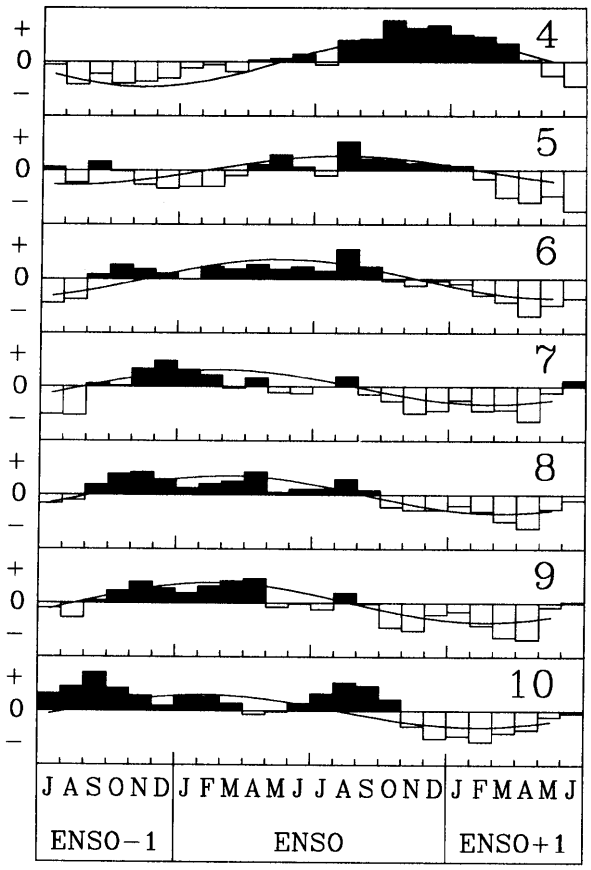

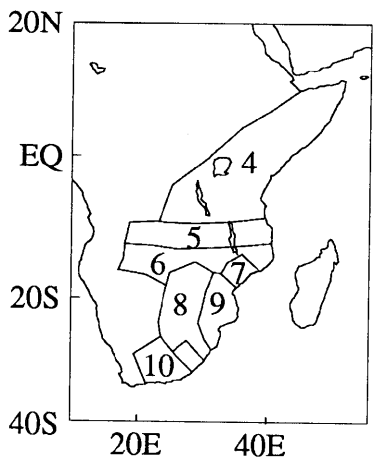

Figure 23. ENSO composite rainfall anomalies (standard departures) for selected sectors in equatorial and southern Africa (from Nicholson and Kim, 1996). Time series commence in July in year −1 and continue to June of the following year. These are roughly arranged from north to south, with the topmost sector just north of the equator and the bottom-most sector situated near 35°S

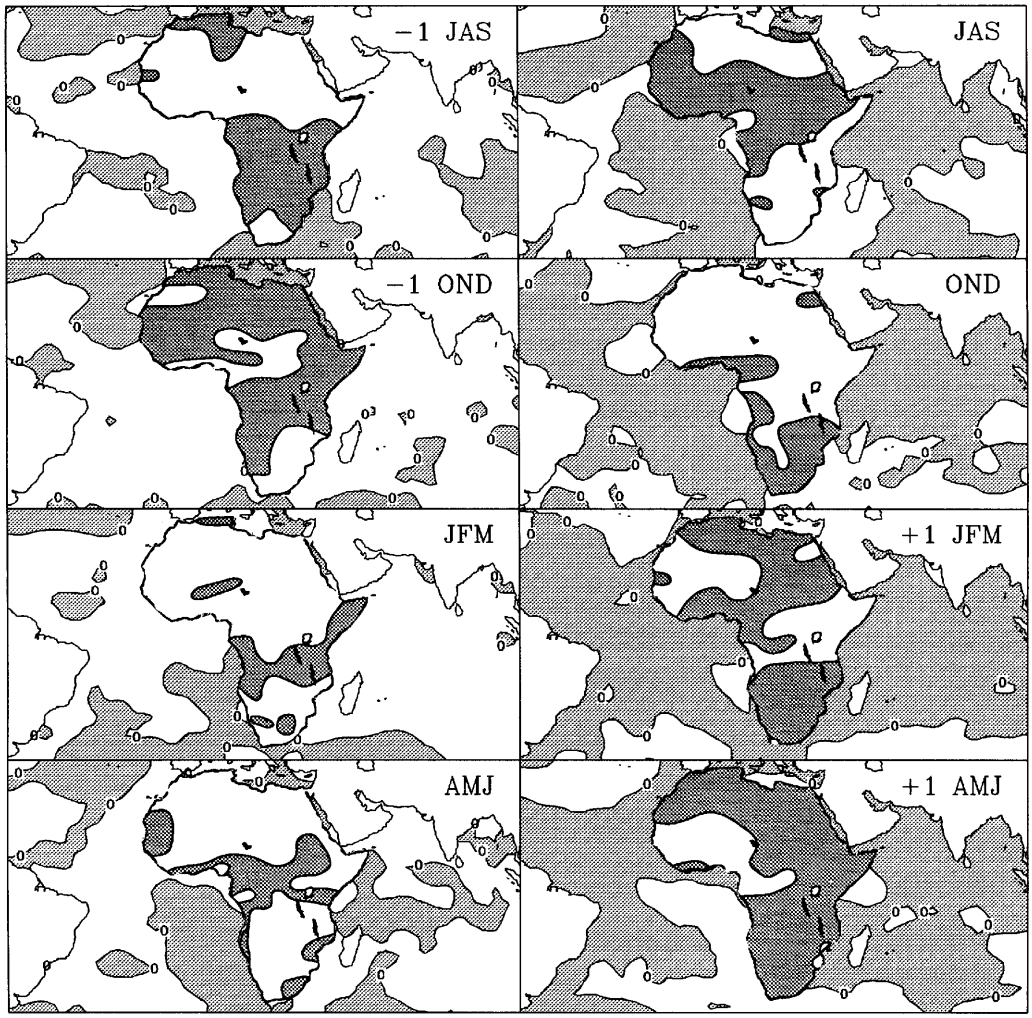

Figure 24. Schematic indicating SST and rainfall anomalies, by season, for the 'cold' and 'warm' phases. For SSTs, positive anomalies are shaded; for rainfall negative anomalies are shaded, in order to emphasize the cold/wet, warm/dry associations. Rainfall is based on Nicholson and Kim (1996)

Maximum cooling in the Atlantic occurs in OND (−1); in the Indian Ocean it occurs during the following JFM. Maximum warming occurs late in the Pacific ENSO cycle, OND of year 0 in the Atlantic and JFM of the following in the Indian Ocean. In the Atlantic the cool phase occurs with greater consistency, whereas in the Indian Ocean the warm phase occurs with greater consistency.

These phases correspond roughly to 'wet' and 'dry' phases over most of the African continent. The ENSO signal in the Atlantic occurs more consistently during the cool phase. In African rainfall and in Indian Ocean SSTs it occurs more consistently during the warm phase. During the cold phase, the ENSO signal in rainfall 'propagates' northward from southern to equatorial Africa; a remarkably similar phase shift in SSTs occurs over the southern and equatorial Atlantic at the same time. During the warm phase, the timing of the rainfall signal is relatively constant from sector to sector, as is the timing of the ENSO signal in SSTs over the Indian Ocean. This and other evidence suggests the possibility that the dominant control on rainfall over Africa switches from the Atlantic during the cold phase to the Indian Ocean during the warm phase. Overall our results strongly indicate that the ENSO signal in rainfall is manifested via ENSO's influence on SSTs in these oceans, which in turn modulate the interannual variability of rainfall over Africa.

The mechanisms of the ENSO signal in the Atlantic and Indian Ocean are beyond the scope of this work. However, the results of this study suggest the possibility that there the ENSO modes in these two oceans are decoupled, so that separate mechanisms may be involved. The diverse spectral characteristics of sectors within the Atlantic (Figure 17(a)), further suggest that various parts of the Atlantic may likewise show independent links to ENSO, particularly the sector north of the ITCZ. There a link to ENSO via the North Atlantic Oscillation is a possibility. Elsewhere both equatorial and extra-tropical Southern Hemisphere teleconnections may be involved.

The consistent temporal relationships between warm episodes in the tropical Atlantic/western Indian Oceans and Pacific ENSO provide forecast potential for the Atlantic–Africa–Indian Ocean sector of the tropics and subtropics. For this potential to be realized, the conditions under which ENSO influences the Atlantic and western Indian Oceans and the dynamic mechanisms linking these sectors with the Pacific must be identified.

ACKNOWLEDGEMENTS

This work was carried out with the support of NOAA Grant NA89AA-D-AC203 and NSF Grants ATM-9024340 and ATM-9024340. The author would like to thank J.-Y. Kim for his assistance in the preparation of figures utilized in the article. The comments and suggestions of Jerry Meehl were extremely useful in producing the final manuscript.

REFERENCES

Aceituno, P. 1988. 'On the functioning of the Southern Oscillation in the South American sector. Part I: surface climate', *Mon. Wea. Rev.*, **116**, 505–524.

Allen, R. J., Lindesay, J. A. and Reason, C. J. C. 1995. 'Multidecadal variability in the climate system over the Indian Ocean region during Austral summer', *J. Climate*, **8**, 1853–1873.

Arkin, P. A. 1982. 'The relationship between interannual variability in the 200 mb tropical wind field and the Southern Oscillation', *Mon. Wea. Rev.*, **110**, 808–823.

Bakun, A. 1978. 'Guinea current upwelling', *Nature*, **271**, 147–150.

Barnett, T. P. 1983. 'Interaction of the monsoon and Pacific tradewind system at interannual timescales. Part I. The equatorial zone', *Mon. Wea. Rev.*, **111**, 756–773.

Brier, G. 1978: 'The quasi-biennial oscillation and feedback processes in the atmosphere–ocean–earth system', *Mon. Wea. Rev.*, **106**, 938–946.

Cadet, D. L. 1985. 'The Southern Oscillation over the Indian Ocean', *J. Climatol*, **5**, 189–212.

Cardone, V. J., Greenwood, J. G. and Cane, M. A. 1990. 'On trends in historical marine wind data', *J. Climate*, **3**, 113–127.

Covey, D. L. and Hastenrath, S. 1978. 'The Pacific El Niño phenomenon and the Atlantic circulation', *Mon. Wea. Rev*, **106**, 1280–1286.

Deser, C. and Blackmon, M. 1993: 'Surface climate variations over the North Atlantic Ocean during winter: 1900–1989', *J. Climate*, **6**, 1743–1753.

Deser, C. and Wallace, J. M. 1990. 'Large-scale atmospheric circulation features of warm and cold episodes in the tropical Pacific', *J. Climate*, **3**, 1254–1281.

Fu, C., Diaz, H. F. and Fletcher, J. O. 1986. 'Characteristics of the response of SST in the central Pacific associated with warm episodes of the Southern Oscillation', *Mon. Wea. Rev.*, **114**, 1716–1738.

Gill, A. E. and Rasmusson, E. M. 1983. 'The 1982–83 climate anomaly in the equatorial Pacific', *Nature*, **306**, 229–234.

Gillooly, J. F. and Walker, N. D. 1984. 'Spatial and temporal behaviour of sea-surface temperatures in the South Atlantic', *S. Afr. J. Sci.*, **80**, 97–100.

Graham, N. E. 1994. 'Decadal-scale climate variability in the tropical and North Pacific during the 1970s and 1980s: observations and model results', *Climate Dyn.*, **10**, 135–162.

Gutzler, D. S. and Harrison, D. E. 1987. 'The structure and evolution of seasonal wind anomalies over the near-equatorial eastern Indian and western Pacific Oceans', *Mon. Wea. Rev.*, **115**, 169–192.

Hamilton, K. and Allingham, A. M. 1988. 'A note on equatorial Atlantic sea surface temperature variations 1890–1979', *Atmos. Ocean*, **26**, 666–678.

Hastenrath, S. 1984. 'Interannual variability and the annual cycle: mechanisms of circulation and climate in the tropical Atlantic sector', *Mon. Wea. Rev.*, **112**, 1097–1107.

Hastenrath, S. and Heller, L. 1977. 'Dynamics of climatic hazards in northeast Brazil', *Q. J. R. Meteorol. Soc.*, **103**, 77–92.

Hisard, P. 1980. 'Observation de réponses de type El Niño dans l'Atlantique tropical oriental Golfe de Guinée', *Oceanol. Acta*, **1**, 69 78.

Hisard, P. and Henin, C. 1987. 'Response of the equatorial Atlantic Ocean to the 1983–84 winds', *J. Geophys. Res.*, **92**, 3759–3768.

Horel, J. D. and Wallace, J. M. 1981. 'Planetary-scale atmospheric phenomena associated with the Southern Oscillation', *Mon. Wea. Rev.*, **109**, 813–829.

Horel, J. D., Kousky, V. E. and Kagano, M. T. 1986. 'Atmospheric conditions in the Atlantic sector during 1983 and 1984', *Nature*, **322**, 248–251.

Houghton, R. W. and Tourre, Y. M. 1992. 'Characteristics of low-frequency sea surface temperature fluctuations in the tropical Atlantic', *J. Climate*, **5**, 765–771.

Katz, E. J., Hisard, P., Verstraete, J. M. and Garzoli, S. L. 1986. 'Annual change of sea surface slope along the equator of the Atlantic Ocean in 1983 and 1984', *Nature*, **222**, 245–247.
Kiladis, G. N. and Diaz, H. F. 1989. 'Global climatic anomalies associated with extremes in the Southern Oscillation', *J. Climate*, **2**, 1069–1090.
Lamb, P. J., Peppler, R. A. and Hastenrath, S. 1986. 'Interannual variability in the tropical Atlantic', *Nature*, **322**, 238–240.
Lau, K.-M. and Sheu, P. J. 1988. 'Annual cycle, quasi-biennial oscillation, and Southern Oscillation in global precipation', *J. Geophys. Res.*, **93**, 10975–10988.
Lindesay, J. A., Harrison, M. S. J. and Haffner, M. P. 1986. 'The Southern Oscillation and South African rainfall', *S. Afr. J. Sci.*, **82**, 196–198.
Mechoso, C. and Lyons, S. 1988. 'On the atmospheric response to SST anomalies associated with the Atlantic warm event during 1984', *J. Climate*, **1**, 422–428.
Meehl, G. A. 1987. 'The annual cycle and interannual variability in the tropical Pacific and Indian Ocean regions', *Mon. Wea. Rev.*, **115**, 27–50.
Meehl, G. A. 1993. 'A coupled air–sea biennial mechanism in the tropical Indian and Pacific regions: role of the oceans', *J. Climate*, **6**, 31–41.
Merle, J. and Arnault, S. 1985. 'Seasonal variability of the surface dynamic topography in the tropical Atlantic Ocean', *J. Marine Res.*, **43**, 267–288.
Merle, J., Fieux, M. and Hisard, P. 1979. 'Annual signal and interannual anomalies of sea surface temperature in the eastern equatorial Atlantic Ocean', *Deep-Sea Res.*, **26**, 77–102.
Michelchen, N. 1985a. 'The Southern Oscillation and the interannual upwelling variations off northwest Africa and in the Gulf of Guinea', *Trop. Ocean Atmos. Newsl.*
Michelchen, N. 1985b. 'About inter-annual coastal upwelling variations off NW-Africa with reference to changes of Southern Oscillation' *International Symposium on Upwelling in Western Africa*, Institute Inv. Pesq., Barcelona, Vol. 1, pp. 93–100.
Molinari, R. L., Battisti, D., Bryan, K. and Walsh, J. 1994. 'The Atlantic Climate Change Program' *Bull. Am. Meteorol. Soc.*, **75**, 1191–1199.
Moore, D. W., Hisard, P., McCreary, J. P., Merle, J., O'Brien, J. J., Picaut, J., Verstraete, J. M. and Wunsch, C. 1978. 'Equatorial adjustment in the eastern Atlantic', *Geophys. Res. Lett.*, **5**, 637–640.
Nicholls, N. 1979. 'Air–sea interaction and the quasi-biennial oscillation', *Mon. Wea. Rev.*, **106**, 1404–1508.
Nicholls, N. 1979. 'A simple air–sea interaction model', *Q. J. R. Meteorol. Soc.*, **105**, 93–105.
Nicholls, N. 1984. 'The Southern Oscillation and Indonesia sea surface temperature', *Mon. Wea. Rev.*, **112**, 424–432.
Nicholson, S. E. and Entekhabi, D. 1986. 'The quasi-periodic behaviour of rainfall variability in Africa and its relationship to the Southern Oscillation', *J. Clim. Appl. Meteorol.*, **34**, 311–348.
Nicholson, S. E. and Entekhabi, D. 1987. 'Rainfall variability in temperatures along the southwestern coast of Africa', *J. Clim. Appl. Meteorol.*, **26**, 561–578.
Nicholson, S. E. and Kim, J. 1997. 'The relationship of the El Niño–Southern Oscillation to African rainfall' *Int. J. Climatol.*, **17**, 117–135.
Nicholson, S. E. and Nyenzi, B. S. 1990. Temporal and spatial variability of SSTs in the tropical Atlantic and Indian Oceans', *Arch. Meteorol. Geophys. Bioklimatol.*, Series A, **42**, 1–17.
Nicholson, S. E., Nyenzi, B. S. and Cooper, H. 1988. 'Interannual variability in the Atlantic and Indian Oceans and its relationship to the Southern Oscillation', *Twelfth Climate Diagnostics Workshop*, National Oceanic and Atmospheric Administration, pp. 114–125.
Nigam, S. and Shen, H.-S. 1993. 'Structure of oceanic and atmospheric low-frequency variability over the tropical Pacific and Indian Oceans. Part I: COADS observations', *J. Climate*, **6**, 657–676.
O'Brien, J. J., Adamec, D. and Moore, D. W. 1978. 'A simple model of upwelling in the Gulf of Guinea', *Geophys. Res. Lett.*, **5**, 641–644.
Philander, S. G. H. 1986. 'Unusual conditions in the tropical Atlantic Ocean in 1984', *Nature*, **222**, 236–238.
Quinn, W. H., Zopf, D. O., Short, K. S. and Kuo Yang, R. T. W. 1978. 'Historical trends and statistics of the Southern Oscillation, El Niño, and Indonesian droughts', *Fish. Bull.*, **76**, 663–678.
Rasmusson, E. M. and Carpenter, T. H. 1982. 'Variations in tropical sea surface temperature and surface wind fields associated with the Southern Oscillation', *Mon. Wea. Rev.*, **110**, 354–384.
Rasmusson, E. M. and Mo., K. 1993. 'Linkages between 200-mb tropical and extratropical circulation anomalies during the 1986 –89 ENSO cycle', *J. Climate*, **6**, 595–616.
Rasmusson, E. M., Wang, X. and Ropelewski, C. F. 1990. 'The biennial component of ENSO variability', *J. Mar. Sys.*, **1**, 71–90.
Ropelewski, C. F. and Halpert, M. S. 1986. 'North American precipitation and temperature patterns associated with the El Niño/Southern Oscillation (ENSO)', *Mon. Wea. Rev.*, **114**, 2352–2362.
Ropelewski, C. F. and Halpert, M. S. 1987. 'Global and regional scale precipitation associated with El Niño/Southern Oscillation', *Mon. Wea. Rev.*, **115**, 985–996.
Ropelewski, C. F. and Halpert, M. S. 1989. 'Precipitation patterns associated with the high index phase of the Southern Oscillation', *J. Climate*, **2**, 268–284.
Ropelewski, C. F. and Jones, P. D. 1987. 'An extension of the Tahiti–Darwin Southern Oscillation Index', *Mon. Wea. Rev.*, **115**, 2161–2165.
Ropelewski, C. F., Halpert, M. S. and Wang, X. 1992. 'Observed tropospheric biennial variability and its relationship to the Southern Oscillation', *J. Climate*, **5**, 594–613.
Schonher, T. and Nicholson, S. E. 1989. 'The relationship between California rainfall and ENSO events', *J. Climate*, **2**, 1258–1269.
Semazzi, F. H. M., Mehta, V. and Sud, Y. C. 1988. 'An investigation of the relationship between sub-Saharan rainfall and global sea surface temperatures', *Atmos. Ocean*, **26**, 118–138.
Servain, J. and Legler, D. M. 1986. 'Empirical orthogonal function analyses of tropical Atlantic sea surface temperature and windstress: 1964–1979', *J. Geophys. Res.*, **91**, 14181–14191.
Servain, J., Picault, J. and Merle, J. 1982. 'Evidence of remote forcing in the equatorial Atlantic Ocean', *J. Phys. Ocean.*, **12**, 457–463.
Shannon, L. V. 1985. 'The Benguela ecosystem, Part I. Evolution of the Benguela, physical features and processes', *Ocean. Mar. Biol. Ann. Rev.*, **23**, 105–182.
Shannon, L. V., Boyd, A. J., Brundrit, G. B. and Taunton-Clark, J. 1986. 'On the existence of an El Niño type phenomenon in the Benguela system', *J. Mar. Res.*, **44**, 495–520.
Tourre and White, 1995. 'ENSO signals in global upper-ocean temperature', *J. Phys. Ocean*, in press.
Van Heerden, J. 1988. 'The Southern Oscillation and South African summer rainfall', *J. Climatol*, **8**, 577–597.

Van Loon, H. 1984. 'The Southern Oscillation. Part III: associations with the trades and with the trough in the westerlies of the South Pacific Ocean', *Mon. Wea. Rev.*, **112**, 94–954.
Van Loon, H. and Shea, D. J. 1985. 'The Southern Oscillation. Part IV: the development of warm and cold events', *Mon. Wea. Rev.*, **113**, 2063–2074.
Walker, N. D. 1987. 'Interannual sea surface temperature variability and associated atmospheric forcing within the Benguela system', Payne, A. I. L., Gulland, J. A. and Brink, K. H. (eds), *The Benguela and Comparable Ecosystems, S. Afr. J. Mar. Sci.*, **5** (special issue), 121–132.
Walker, N. D. 1990. 'Links between South African summer rainfall and temperature variability of the Agulhas and Benguela current systems', *J. Geophys. Res.*, **95** 3297–3319.
Walker, N. D., Taunton-Clark, J. and Pugh, J. 1984. 'Sea temperatures off the South African west coast as indicators of Benguela warm events', *S. Af. J. Sci.*, **80** 72–77.
Ward, M. N. 1992. 'Provisionally corrected surface wind data, worldwide ocean–atmosphere surface fields and Sahelian rainfall variability', *J. Climate*, **5** 454–475.
Wolter, K. 1987. 'The Southern Oscillation in surface circulation and climate over the tropical Atlantic, eastern Pacific, and Indian Oceans as captured by cluster analysis', *J. Clim. Appl. Meteorol.*, **26** 540–558.
Woodruff, S. D., Slutz, R. J., Jenne, R. L. and Steurer, P. M. 1987. 'A comprehensive ocean–atmosphere data set ', *Bull. Am. Meteorol. Soc.*, **68** 1239–1250.
Yasunari, T. 1985. 'Zonally propagating modes of the global east–west circulation associated with the Southern Oscillation', *J. Meteorol. Soc. J.*, **63** 1013–1029.
Yasunari, T. 1987a. 'Global structure of the El Niño/Southern Oscillation. Part I. El Niño composites ', *J. Meteorol. Soc. J.*, **65** 67–80.
Yasunari, T. 1987b. 'Global structure of the El Niño/Southern Oscillation. Part II. Time evolution', *J. Meteorol. Soc. J.*, **65** 81–102.
Zebiak, S. E. 1993. 'Air–sea interaction in the equatorial Atlantic region', *J. Climate*, **6** 1567–1586.